Active Atmosphere-Ecosystem Exchange of the Vast Majority of Detected Volatile Organic Compounds

J.-H. Park *et al.*

Science **341**, 643 (2013);
DOI: 10.1126/science.1235053

Science (print ISSN 0036-8075; online ISSN 1095-9203) is published weekly, except the last week in December, by the American Association for the Advancement of Science, 1200 New York Avenue NW, Washington, DC 20005.

beyond the endurance of 10^6 for the conventional FG memory cell. Moreover, the measured disturb margin of this device met the requirements of memory array operation (fig. S7).

Compared with 6T-SRAM, the transistor number is reduced to one with the SFG memory cell, whereas the speed is comparable. As a result, the unit memory cell size and the cost of the chip can be greatly reduced. The power consumption would also be greatly reduced, because the write current is below 1 μA. For comparison, the 1T1C DRAM cell needs a write current of over 10 μA to quickly charge and discharge the capacitor of 25 fF (*14*).

When the pn junction between the SFG and D of a SFG transistor was exposed to light, the photogenerated carriers induced a tiny photocurrent. As indicated in the device symbol shown in Fig. 4A, the V_{th} of the SFG transistor will change accordingly when the photogenerated carriers are collected by the SFG. The SFG device can then be modified for light sensing by enlarging the area of the photodiode for better light sensitivity. Using the image-sensing SFG transistor, an imaging array was configured (fig. S8). The imaging function of the SFG transistor was evaluated by setting V_{CG} to 0 V during light exposure, using photocurrent as the major writing-1 mechanism. It can be seen from Fig. 4B that a single device has different threshold voltages when it is exposed to different light intensities. The SFG transistor locally amplifies the photogenerated current to a large change in D current for each transistor, whereby the active pixel image-sensing function is realized. In Fig. 4C, the SFG transistor was operated in the image-sensing operation mode, with a sequence of "reset - exposure - read". During the reset operation, the SFG was initialized to a low potential by a reset pulse of $V_{CG} = 2$ V and $V_D = -1$ V. During the exposure stage, the pn junction between SFG and D was reverse-biased and V_{CG} was set to 0 V. After an exposure operation of 20 ms, a reading operation was executed with $V_{CG} = 1.28$ V and $V_D = 1.5$ V. The readout D current of the reading operation is summarized in Fig. 4D. The D current at the reading operation increases linearly with the increasing light intensity from 109 to 4090 lux. Thus, an active pixel image sensor (APS) function was realized with a single SFG cell. For comparison, the CMOS image-sensing technology uses three MOSFETs plus a photodiode to compose a functional APS. Using the SFG cell as an APS cell, the pixel density of the image-sensing chip can be increased, and the reading operation becomes nondestructive.

As an emerging fundamental semiconductor device, the SFG transistor concept opens up possibilities for innovations for many technologies, such as DRAM, SRAM, TFET, and APS. The SFG transistor may become a fundamental semiconductor device after MOSFET (*15*) and FG-MOSFET (*16*), given its merits such as ultra–high-speed memory function and an active image-sensing function.

References and Notes

1. M. Ieong, B. Doris, J. Kedzierski, K. Rim, M. Yang, *Science* **306**, 2057–2060 (2004).
2. Y. Taur, *IEEE Spectr.* **36**, 25–29 (1999).
3. A. Heinrich, S. Loth, *Science* **332**, 1039–1040 (2011).
4. A. Makarov, V. Sverdlov, S. Selberherr, *Microelectron. Reliab.* **52**, 628–634 (2012).
5. J. Koga, A. Toriumi, *IEEE Electron Device Lett.* **20**, 529–531 (1999).
6. C. Aydin *et al.*, *Appl. Phys. Lett.* **84**, 1780–1782 (2004).
7. W. Hansch, C. Fink, J. Schulze, I. Eisele, *Thin Solid Films* **369**, 387–389 (2000).
8. C. Anghel, A. Hraziia, A. Gupta, A. Amara, A. Vladimirescu, *IEEE Trans. Electron. Dev.* **58**, 1649–1654 (2011).
9. A. M. Ionescu, H. Riel, *Nature* **479**, 329–337 (2011).
10. Materials and methods are available as supplementary materials on *Science* Online.
11. E. O. Kane, *J. Phys. Chem. Solids* **12**, 181–188 (1960).
12. P.-F. Wang *et al.*, *Solid-State Electron.* **48**, 2281–2286 (2004).
13. K.-H. Kao *et al.*, *IEEE Trans. Electron. Dev.* **59**, 2070–2077 (2012).
14. I.-G. Kim, S.-H. Park, J.-S. Yoon, D.-J. Kim, J.-Y. Noh, *et al.*, *IEDM Tech. Dig.* **13**, 319–322 (2005).
15. C. Hu, *Modern Semiconductor Devices for Integrated Circuits* (Pearson Education, Upper Saddle River, NJ, ed. 1, 2009).
16. D. Kahng, S. M. Sze, *Bell Syst. Tech. J.* **46**, 1288–1295 (1967).

Acknowledgments: This research was partially supported by the National Natural Science Foundation of China (grant no. 61176074), the National Science and Technology Major Project of China (grant no. 2009ZX02039-003), and the Key Technologies Research and Development Program of Jiangsu Province (grant no. BE2009055, SISPARK). The authors are grateful to M.-F. Li, S.-J. Ding, and A.-Q. Jiang (Fudan University) for discussions on device concepts and measurements.

Supplementary Materials

www.sciencemag.org/cgi/content/full/341/6146/640/DC1
Materials and Methods
Figs. S1 to S8
References

23 May 2013; accepted 27 June 2013
10.1126/science.1240961

Active Atmosphere-Ecosystem Exchange of the Vast Majority of Detected Volatile Organic Compounds

J.-H. Park,[1,2]* A. H. Goldstein,[1,3]† J. Timkovsky,[2] S. Fares,[1,4] R. Weber,[1] J. Karlik,[5] R. Holzinger[2]

Numerous volatile organic compounds (VOCs) exist in Earth's atmosphere, most of which originate from biogenic emissions. Despite VOCs' critical role in tropospheric chemistry, studies for evaluating their atmosphere-ecosystem exchange (emission and deposition) have been limited to a few dominant compounds owing to a lack of appropriate measurement techniques. Using a high–mass resolution proton transfer reaction–time of flight–mass spectrometer and an absolute value eddy-covariance method, we directly measured 186 organic ions with net deposition, and 494 that have bidirectional flux. This observation of active atmosphere-ecosystem exchange of the vast majority of detected VOCs poses a challenge to current emission, air quality, and global climate models, which do not account for this extremely large range of compounds. This observation also provides new insight for understanding the atmospheric VOC budget.

About 90% of atmospheric volatile organic compounds (VOCs) originate from biogenic sources (BVOCs) (*1*). VOCs play a critical role in tropospheric chemistry and are associated with ozone production and secondary organic aerosol (SOA) formation, which affect human health, regional air quality, and the global climate (*2–4*). Once VOCs are emitted, they either undergo oxidation until they form carbon dioxide, deposition to a surface, or transformation into SOAs (*5*). A few studies have shown that unmeasured BVOCs were responsible for O_3 chemical loss and missing OH reactivity (*6–8*). Previous BVOC flux field observations mainly focused on a few dominant BVOCs such as methanol, isoprene, and terpenes, and the number of compounds for which fluxes could be simultaneously measured was generally limited to 18 compounds (*9*). Owing to technical measurement limitations, understanding of VOC deposition remains limited, yet this loss process may dominate the removal of atmospheric VOCs (*5*, *10*). Deposition of only a few oxygenated VOCs (OVOCs) has been previously observed in forests (*11*).

[1]Department of Environmental Science, Policy, and Management, University of California at Berkeley, Berkeley, CA 94720, USA. [2]Institute for Marine and Atmospheric Research Utrecht, Princetonplein 5, 3584 CC, Utrecht, Netherlands. [3]Department of Civil and Environmental Engineering, University of California at Berkeley, Berkeley, CA 94720, USA. [4]Consiglio per la ricerca e la sperimentazione in agricoltura–Research Center for the Soil-Plant System, Rome, Italy. [5]University of California Cooperative Extension, Bakersfield, CA 93307, USA.

*Present address: Institute of Arctic and Alpine Research (INSTAAR), University of Colorado at Boulder, Boulder, CO 80309, USA.
†Corresponding author. E-mail: ahg@berkeley.edu

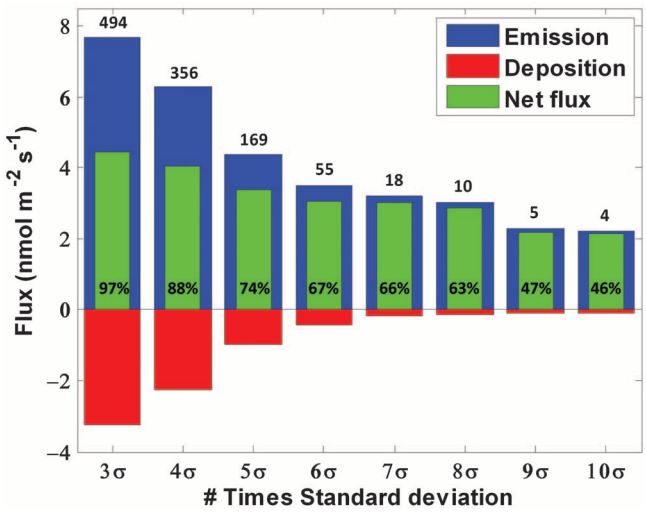

Fig. 1. Flux contribution by identified ions that had a flux exceeding S/N of three or more. Sigma (σ) indicates standard deviation of the noise. Blue, red, and green bars indicate the estimated 24-hour mean total emission, estimated 24-hour mean total deposition, and observed 24-hour mean net exchange, respectively. The number of ions in each bin is indicated above. The percentage shown in the green bars indicates the flux contribution to total net flux of 555 ions on a molar basis.

We present results of direct flux measurement over an orange grove in California's Central Valley during the summer of 2010 (*12*). We used a proton transfer reaction–time of flight–mass spectrometer (PTR-TOF-MS) (*13*, *14*), collected VOC concentration data at 5 Hz, and evaluated the data using the eddy-covariance (EC) method. We calculated mixing ratios and fluxes for 555, mostly organic, ions with mass-to-charge ratios (*m/z*) between 31 and 1263 (hereafter referred to as "ions"), as described by Holzinger *et al*. (*15*). The detection of fluxes for ions that are only emitted or only deposited is straightforward, but determination of fluxes for ions that experience both emission and deposition and for which the net flux is small is more challenging. The flux detection method that we used computes the "absolute value" of covariance between measured vertical wind speed and ion-mixing ratios, effectively adding absolute value signals for emis-

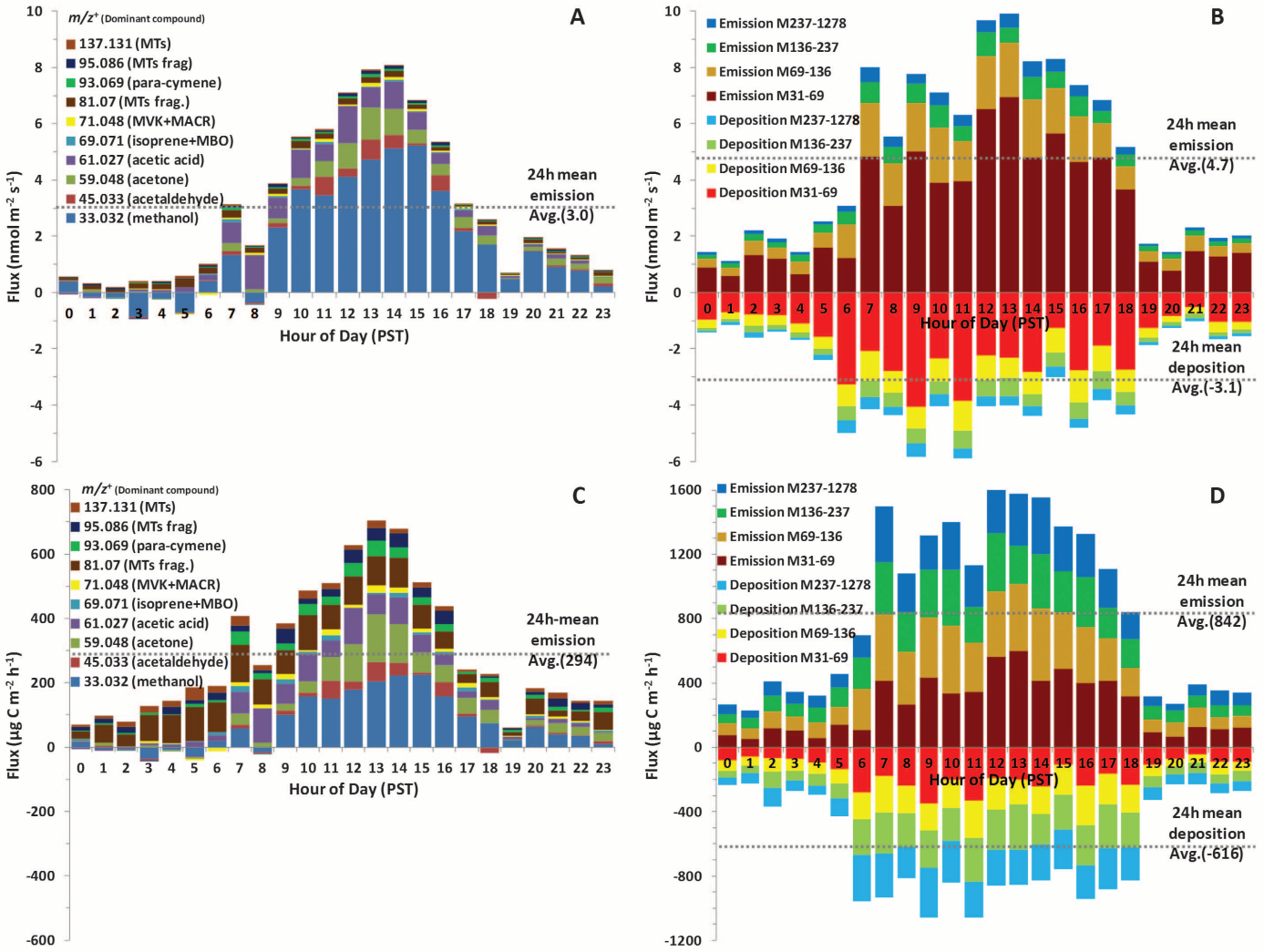

Fig. 2. BVOC diurnal emission and deposition fluxes. On a molar basis for (**A**) 10 major compounds, (**B**) four different mass ranges categorized as *m/z* 31-69 (*n* = 61), *m/z* 69-136 (*n* = 141), *m/z* 136-237 (*n* = 141), and *m/z* 237-1278 (*n* = 141), and on a carbon mass basis for (**C**) 10 major masses and (**D**) four classes. Staged bar plots of 10 masses and four classes with the largest fluxes are shown as diurnal cycles with *m/z* (or *m/z* range) indicated in the legend. The scale of the *y* axis in (C) is half that of (D).

sion and deposition to more easily detect when bidirectional exchange is occurring (*16*). Noise levels (N) were computed in the same way but with vertical wind data that were time shifted. The measured ions were categorized by their signal-to-noise ratios (S/N), and the detection limit for flux was defined as S/N ≥ 3. Of the 555 ions analyzed, 494 ions (~89%) passed the S/N = 3 filter. Figure 1 shows the number of ions that passed this and more stringent filters (S/N = 4 to 10).

The net flux was calculated by EC for all ions. On a molar basis, the net flux (Fig. 1, green bars) of 494 ions contributed 97% of the total net flux of 4.43 nmol m^{-2} s^{-1} for all 555 ions observed. Deposition for ions above S/N = 3 was substantial, with a total magnitude of –3.24 nmol m^{-2} s^{-1}, which is 42% of the total emission of ions above S/N = 3, and exceeding the total emission of 3.03 nmol m^{-2} s^{-1} of the 10 ions that passed the S/N = 8 filter and constitute the 10 dominant BVOC fluxes measured. This result supports the idea that many unexplored VOCs exist in the atmosphere and are actively exchanged with ecosystems (*5*, *10*).

Most BVOC flux field observations only measure the dominant VOCs that are included in our top 10 major compounds exceeding S/N = 8. These dominant compounds were almost exclusively emitted throughout the day, except for small deposition of a few compounds in the early morning and evening (Fig. 2A). The 24-hour mean net flux of these 10 major compounds contributed 63% to the observed total (Figs. 1 and 2A). We classified all other 484 ions above S/N = 3 (but below S/N = 8) into four groups by size, including *m/z* ranges of M31-69 (*n* = 61 observed), M69-136 (*n* = 141), M136-237 (*n* = 141), and M237-1278 (*n* = 141), respectively. The *m/z* of 237 has been previously observed in the gas phase by PTR-MS as a β-caryophyllene oxidation product (*17*); however, none of the other ions in the group M237-1278 has been reported before. The results for compounds in this group are uncertain because they are less volatile and sticky and are currently not well understood. Thus, further research in this *m/z* range is recommended. All 484 of these ions were observed to have fluxes that were bidirectional throughout the day (Fig. 2B). Both emission and deposition fluxes were at their maxima during daytime; by contrast, the concentrations were generally lower during day and higher at night owing to buildup in the shallow nighttime boundary layer (table S2) (*16*). Although their 24-hour mean total net flux was an emission (1.61 nmol m^{-2} s^{-1}) and smaller than the total net emission of the summed 10 major compounds (2.82 nmol m^{-2} s^{-1}) described above, their 24-hour mean estimated emission was ~1.6 times as large as that of the 10 major compounds. Their 24-hour mean estimated deposition was of similar magnitude to the net emission of the 10 major compounds (Fig. 2, A and B, and table S1) (*16*). A 24-hour mean net deposition occurred for 186 ions, but no single ions accounted for more than 1.6% of the total estimated deposition on a molar basis.

We did not find any ions depositing uniformly throughout the day. More ions with net deposition were observed in the higher *m/z* group (Fig. 3 and table S1) (*16*), suggesting that heavier (presumably lower vapor pressure) molecules deposit more efficiently. For the 186 ions observed to have net deposition, the exchange velocity (or deposition velocity) was calculated

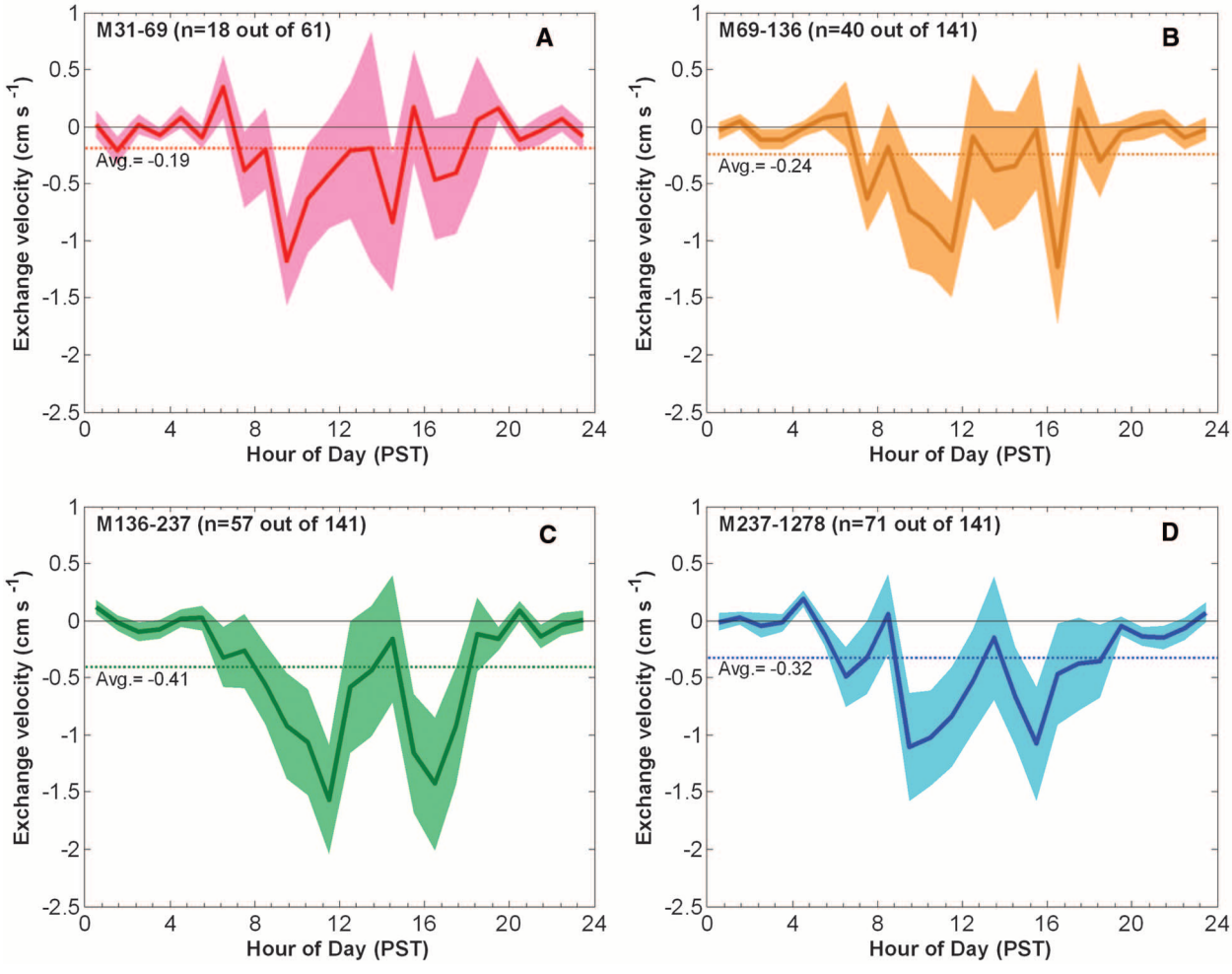

Fig. 3. Mean diurnal cycle of exchange velocity for depositing species in *m/z* categories. Range 31-69 (**A**), 69-136 (**B**), 136-237 (**C**), and 237-1278 (**D**). Dotted lines indicate the 24-hour mean exchange velocity for each group; the shaded area indicates SEM.

according to V_{ex} = flux/ambient concentration, and the diurnal trends were examined (*16*). On the basis of this analysis, a 24-hour mean V_{ex} in M136-237 of –0.41 cm s^{-1} was the fastest deposition rate, and the maximum hourly deposition was between –1 and –1.5 cm s^{-1} for all groups. During daytime, two V_{ex} minima usually appeared, first in the morning hours from 09:00 to 12:00 PST and second in the afternoon hours from 14:00 to 17:00 PST. Surprisingly, slower V_{ex} in the hours from 12:00 to 15:00 was observed for all groups (Fig. 3). This implies that direct emission from the ecosystem and/or within-canopy photochemical production reduces the net deposition when both temperature and sunlight intensity are at a maximum. Recently, Karl *et al.* (*11*) observed deposition of methyl vinyl ketone (MVK) and methacrolein (MACR) and a few other OVOCs, including acetaldehyde, to deciduous forests, but those accounted for only a small fraction of what we observed as deposition. In contrast to Karl *et al.*'s results, we observed MVK and MACR to have bidirectional flux that resulted in net emission. For these compounds, we unambiguously observed emissions during daytime, with small deposition in the early morning, and found excellent agreement with vertical gradient observations performed simultaneously at the site using a separate instrument (fig. S2) (*16*). The exchange velocity range we observed for the 186 depositing ions (Fig. 3) was generally lower or at the low end of the values reported above deciduous forests (*11*).

In contrast to our molar-basis analysis above, when considering carbon mass flux, the heavier ions observed are generally more important. We estimated carbon mass fluxes for each group by conservatively assuming 2, 5, 10, and 15 carbon atoms on average for ions in the groups M31-69, M69-136, M136-237, and M237-1278, respectively. Our estimated carbon emission from the sum of all 484 observed ions (842 μg C m^{-2} $hour^{-1}$) is 2.8 times as large as the sum of the 10 major compounds (294 μg C m^{-2} $hour^{-1}$), and the estimated carbon deposition was twice as large (Fig. 2, C and D) as the net emission of the 10 major compounds, suggesting that carbon mass flux of these 484 ions is even more substantial on a carbon mass basis than on a molar basis. This estimate is conservative and likely an underestimate because more carbons may be expected in each class than the carbon numbers we assumed, and another fraction of carbon is not accounted for owing to fragmentation in the PTR-TOF-MS (*16*). The estimated total emission of the M31-69 group was the largest, and estimated total emissions decreased as the *m/z* group number increased. The deposition was almost equivalent among the four groups except for M69-136, for which the deposition was slightly lower (Fig. 2D and table S1) (*16*).

We used the high–mass resolution molecular weight observations to identify chemical formulas for 162 observed hydrocarbons and oxidized hydrocarbons by selecting the ions exceeding S/N = 3, smaller than *m/z* 237, and consisting of only carbon (C), hydrogen (H), and oxygen (O) atoms within a mass range tolerance of ±3 mD (table S2) (*16*). The 24-hour mean total net flux for these 162 identified ions contributed 77% to the total on a molar basis. Using the molecular formula from 152 ions identified (excluding 10 dominant ions), we calculated carbon mass fluxes and summarized them in groups of pure hydrocarbons (C_xH_y) and oxygenated hydrocarbons containing one, two, and three or more oxygen atoms (i.e., C_xH_yO, $C_xH_yO_2$, $C_xH_yO_{3+}$). A 24-hour mean net emission flux of 426 μg C m^{-2} $hour^{-1}$ was estimated, and the total net flux of 152 ions accounted for about one-third of the total (Fig. 4, left pie chart). Pure hydrocarbons (C_xH_y; n = 40) constituted 15% of the total carbon flux of these 162 ions, and ions containing one to three or more oxygens (C_xH_yO: n = 30; $C_xH_yO_2$: n = 44; and $C_xH_yO_{3+}$: n = 38) contributed 12.7, 3.2, and 1.8%, respectively. Although the summed flux of these 152 ions was a net emission of 139 μg C m^{-2} $hour^{-1}$, it is instructive to look separately at the contributions of oxygenated hydrocarbons and pure hydrocarbons to the estimated total emissions and depositions. For estimated total emission in each category, oxygenated hydrocarbons were dominant, but pure hydrocarbon (C_xH_y) emission was individually the largest, followed by C_xH_yO, $C_xH_yO_2$, and $C_xH_yO_{3+}$, indicating that the vast array of unknown VOCs were either photochemically produced below the measurement height or directly emitted from the ecosystem, and were larger than the emission of the 10 dominant and commonly measured compounds. Thus, this fuller range of compounds provides an extremely important contribution to the total observed emissions (Fig. 4). Moreover, we also estimated greater deposition fluxes for oxygenated hydrocarbons (71%) than for pure hydrocarbons (29%), and $C_xH_yO_2$ deposition exceeded C_xH_y deposition (Fig. 4). This result is consistent with the idea that less-oxygenated VOCs are emitted from the ecosystem, whereas secondary compounds produced through atmospheric photochemical process and containing more oxygen atoms are preferentially removed by dry deposition.

Our results show that the mass balance of VOCs in the orange orchard ecosystem is highly incomplete when considering only emission and deposition of commonly measured dominant

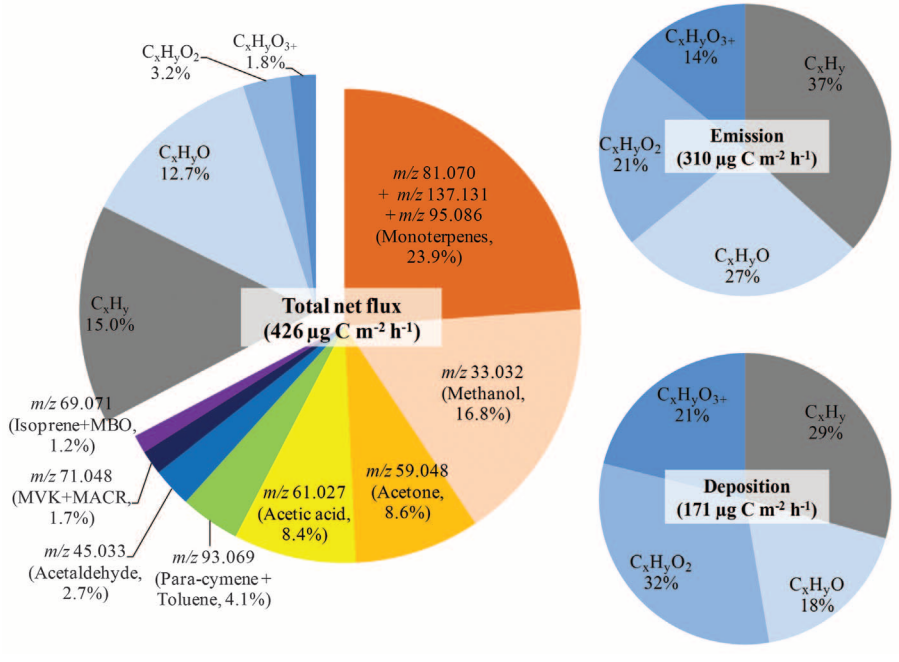

Fig. 4. Flux contribution by chemical composition. Individual VOC and VOC-group contribution to the total flux for ions to which an empirical formula has been attributed (162 ions) are shown in pie chart on the left. The 10 major masses were specifically identified, and the remaining 152 *m/z* ratios were categorized by number of oxygens in the molecule as C_xH_y, C_xH_yO, $C_xH_yO_2$, and $C_xH_yO_{3+}$. The two pie charts on the right show the contribution of categorized ions to the estimated emission (top) and deposition (bottom). MBO, 2-methyl-3-butene-2-ol.

BVOCs. The contribution from hundreds of individually minor compounds is important. Future research is required to determine if this is also true for ecosystems that emit larger quantities of isoprene and/or monoterpenes.

The minor species with lower fluxes and concentrations are not in current BVOC emission models, but their sizes, chemical formulae, and sum suggest that they should be important for SOA formation and regional photochemistry. Their presence in the atmosphere may also account for a sizable amount of the missing OH chemical reactivity and O_3 chemical loss observed in plant environments.

References and Notes

1. A. Guenther *et al.*, *J. Geophys. Res. Atmos.* **100**, 8873 (1995).
2. W. L. Chameides, R. W. Lindsay, J. Richardson, C. S. Kiang, *Science* **241**, 1473–1475 (1988).
3. M. O. Andreae, P. J. Crutzen, *Science* **276**, 1052–1058 (1997).
4. M. S. Jang, N. M. Czoschke, S. Lee, R. M. Kamens, *Science* **298**, 814–817 (2002).
5. A. H. Goldstein, I. E. Galbally, *Environ. Sci. Technol.* **41**, 1514–1521 (2007).
6. M. R. Kurpius, A. H. Goldstein, *Geophys. Res. Lett.* **30**, 1371 (2003).
7. P. Di Carlo *et al.*, *Science* **304**, 722–725 (2004).
8. R. Holzinger, A. Lee, K. T. Paw, A. H. Goldstein, *Atmos. Chem. Phys.* **5**, 67–75 (2005).
9. T. M. Ruuskanen *et al.*, *Atmos. Chem. Phys.* **11**, 611–625 (2011).
10. M. Hallquist *et al.*, *Atmos. Chem. Phys.* **9**, 5155–5236 (2009).
11. T. Karl *et al.*, *Science* **330**, 816–819 (2010).
12. J.-H. Park *et al.*, *Atmos. Chem. Phys.* **13**, 1439–1456 (2013).
13. A. Jordan *et al.*, *Int. J. Mass Spectrom.* **286**, 122–128 (2009).
14. M. Graus, M. Müller, A. Hansel, *J. Am. Soc. Mass Spectrom.* **21**, 1037–1044 (2010).
15. R. Holzinger, A. Kasper-Giebl, M. Staudinger, G. Schauer, T. Rockmann, *Atmos. Chem. Phys.* **10**, 10111–10128 (2010).
16. See supplementary materials on *Science* Online.
17. A. Lee *et al.*, *J. Geophys. Res. Atmos.* **111**, 21 (2006).

Acknowledgments: This work was supported by the Netherlands Organization for Scientific Research (NWO) under the ALW-Middelgroot program (grant 834.08.002), the California Air Resources Board (Award 06-329), the Citrus Research Board, and the University of Utrecht short stay fellowship program. We thank the Gorden Ranch for hosting this study and for the assistance provided by the University of California Lindcove Research and Extension station.

Supplementary Materials

www.sciencemag.org/cgi/content/full/341/6146/643/DC1
Materials and Methods
Figs. S1 to S4
Tables S1 to S3
References (*18*–*28*)

11 January 2013; accepted 2 July 2013
10.1126/science.1235053

Social Influence Bias: A Randomized Experiment

Lev Muchnik,[1] Sinan Aral,[2]* Sean J. Taylor[3]

Our society is increasingly relying on the digitized, aggregated opinions of others to make decisions. We therefore designed and analyzed a large-scale randomized experiment on a social news aggregation Web site to investigate whether knowledge of such aggregates distorts decision-making. Prior ratings created significant bias in individual rating behavior, and positive and negative social influences created asymmetric herding effects. Whereas negative social influence inspired users to correct manipulated ratings, positive social influence increased the likelihood of positive ratings by 32% and created accumulating positive herding that increased final ratings by 25% on average. This positive herding was topic-dependent and affected by whether individuals were viewing the opinions of friends or enemies. A mixture of changing opinion and greater turnout under both manipulations together with a natural tendency to up-vote on the site combined to create the herding effects. Such findings will help interpret collective judgment accurately and avoid social influence bias in collective intelligence in the future.

We rely on ratings contributed by others to make decisions about which hotels, books, movies, political candidates, news, comments, and stories are worth our time and money (*1*). Given the widespread use and economic value of rating systems (*2*–*4*), it is important to consider whether they can successfully harness the wisdom of crowds to accurately aggregate individual information. Do they produce useful, unbiased, aggregate information about the quality of the item being rated? Or, as suggested by the experiments of Salganik *et al.* (*5*), are outcomes path dependent, yielding different aggregate ratings for items of equivalent quality?

Collective intelligence has recently been heralded as a harbinger of accelerated human potential (*6*). But, social influence on individuals' perceptions of quality and value could create herding effects that lead to suboptimal market outcomes (*7*, *8*); rich-get-richer dynamics that exaggerate inequality (*9*–*12*); a group think mentality that distorts the truth (*13*); and measurable disruptions in the wisdom of crowds (*14*). If perceptions of quality are biased by social influence, attempts to aggregate collective judgment and socialize choice could be easily manipulated, with dramatic consequences for our markets, our politics, and our health.

The recent availability of population-scale data sets on rating behavior and social communication enable novel investigations of social influence (*1*, *15*–*20*). Unfortunately, our understanding of the impact of social influence on collective judgment is limited because empirically distinguishing influence from uninfluenced agreement on true quality is nearly impossible in observational data (*21*–*27*). For example, popular products may be popular because of the irrational effect of past positive ratings, or alternatively, the best products may become popular because they are of the highest quality. We must distinguish these explanations to determine the extent to which social influence creates irrational herding.

We therefore designed and analyzed a large-scale randomized experiment to quantify the effects of social influence on users' ratings and discourse on a social news aggregation Web site, where users contribute news articles and discuss them. Users of the site that we studied write comments in response to posted articles, and other users can then "up-vote" or "down-vote" these comments, yielding an aggregate current rating for each posted comment equal to the number of up-votes minus the number of down-votes. Users do not observe the comment scores before clicking through to comments—each impression of a comment is always accompanied by that comment's current score, tying the comment to the score during users' evaluation—and comments are not ordered by their popularity, mitigating selection bias on high (or low) rated comments. Similar scoring mechanisms are widely used on the Web to reward users for supplying insightful or interesting analysis, while penalizing those posting irrelevant, redundant, or low-quality comments. The vast majority of interuser relations occur on the Web site, in contrast to Web sites whose members also interact offline. The data therefore provide a unique opportunity to comprehensively study social influence bias in rating behavior.

Over 5 months, 101,281 comments submitted on the site were randomly assigned to one of three treatment groups: up-treated, down-treated, or control. Up-treated comments were artificially given an up-vote (a +1 rating) upon the comment's creation, whereas down-treated comments were given a down-vote (a –1 rating) upon the comment's creation. Users were unaware of the

[1]School of Business Administration, The Hebrew University of Jerusalem, Mount Scopus, Jerusalem, 91905 Israel. [2]MIT Sloan School of Management, 100 Main Street, Cambridge, MA 20142, USA. [3]NYU Stern School of Business, 44 West 4th Street, New York, NY 10012, USA.

*Corresponding author. E-mail: sinana@mit.edu

Supplementary Materials for

Active Atmosphere-Ecosystem Exchange of the Vast Majority of Detected Volatile Organic Compounds

J.-H. Park, A. H. Goldstein,* J. Timkovsky, S. Fares, R. Weber, J. Karlik, R. Holzinger

*Corresponding author. E-mail: ahg@berkeley.edu

Published 9 August 2013, *Science* **341**, 643 (2013)
DOI: 10.1126/science.1235053

This PDF file includes:

Supporting Online Material

for

Active Atmosphere-Ecosystem Exchange of the Vast Majority of Detected Volatile Organic Compounds

J.-H. Park, A. H. Goldstein*, J. Timkovsky, S. Fares, R. Weber, J. Karlik, R. Holzinger

* Correspondence to: ahg@berkeley.edu

Materials and Methods

1. Measurement site and instruments

An intensive VOC flux measurement field campaign took place in an orange grove in California's Central valley during summer 2010 (24 June to 26 July) as part of a one-year continuous field campaign (Oct. 2009 – Nov. 2010). Details of the site location, environmental conditions, and experimental setup have been described in Fares et al. (*18, 19*), and Park et al. (*12*). Briefly, this area features a Mediterranean-type climate with warm and dry summers. No rain was observed during the measurement period and the temperature remained within the range of 16–40 ^{o}C. Winds were predominantly westerly during the day and easterly at night. During the daytime (10:00 – 14:00 PST; Pacific Standard Time) footprints were mostly (> 90%) within the orchard block of 'Valencia' orange trees (mean tree height ~3.7 m). To measure ambient concentrations of volatile organic compounds (VOC) and their ecosystem-scale fluxes, we deployed a proton transfer reaction-time of flight-mass spectrometer (PTR-TOF-MS) and a quadrupole PTR-MS along with a three-dimensional sonic anemometer. Both PTR instruments use hydronium ions (protonated water, H_3O^+) to chemically ionize the compounds of interest through proton transfer reactions, thus any compound with a proton affinity exceeding that of water can be detected. Detailed descriptions of the instrument and measurement principles have been published elsewhere (for PTR-TOF-MS: (*13, 14*); for PTR-MS: (*20, 21*)). Eddy covariance (EC) fluxes were calculated for the first 0-30 min of every hour, then that 30 minute flux calculation was assumed to be representative of the full hour for

graphical presentations of the diurnal cycles. The EC flux data used here fulfilled stationarity criteria of 70% with tilt angle criteria of ±5° following wind rotation. The EC flux calculation used here has been previously described in detail in Park et al. (*12*). Through an inter-comparison study between the two PTR instruments in addition to spectral analysis of the PTR-TOF-MS flux data (*12*), we concluded that the PTR-TOF-MS is a powerful new tool for quantifying ecosystem fluxes for a wide range of VOC. As an example, figure S2 shows good agreement of the vertical gradients measured by PTR-MS and eddy covariance (EC) flux by PTR-TOF-MS for the sum of methyl-vinyl-ketone and methacrolein (MVK+MACR), but PTR-MS was not used to measure eddy covariance flux of MVK+MACR due to limitations of standard PTR-MS instruments (equipped with a quadrupole mass filter) which allows observation of only a small number of compounds with fast enough time resolution for flux measurements (4 or 5 compounds in 1 second). PTR-MS eddy covariance flux measurements focused on the dominant expected BVOCs.

2. Determination of m/z ratios exchanging with the ecosystem as detected by PTR-TOF-MS

A total of 664 significant mass peaks were identified by analytical software according to Holzinger et al. (*15*). These included major primary ions (e.g. $(H_2O)H^+$, $(H_2O)_2H^+$, $(H_2O)_3H^+$), their isotopes (e.g. $H_2{}^{18}OH^+$, $H_2{}^{16}O{\cdot}H_2{}^{18}OH^+$), impurities such as $O_2{}^+$, NO^+, N_2H^+, ammonium ions (e.g. $NH_3{}^+$, $NH_3NH_3H^+$), and some artifact peaks surrounding the primary ion m/z ratios which were caused by the high ion abundance at the primary ion signal. After excluding all above mentioned peaks, we applied the flux calculation routines described in Park et al (*12*) to the remaining 555 peaks above *m/z* 31 (this includes protonated CH_2OH^+). In the following we outline the method applied to determine whether compounds represented by these ions were exchanged between the atmosphere and the ecosystem. This is a non-trivial analysis especially for compounds with bi-directional or small fluxes. The analysis presented below was done using lag-time corrected VOC data. Lag-time correction is described in Park et al. (*12*) and accounts for

the transport time in the tubing and time-shifts between different computer clocks that were used to record PTR-TOF-MS data and wind data, respectively.

As a first step, we investigated co-variances of vertical wind speed with VOC data using the following procedure: (i) within the limits of ± 180 seconds, we shifted the wind data in steps of 0.2 s; (ii) we calculated the absolute value of the covariance between VOC data and time-shifted wind data, effectively disregarding the sign of the flux; (iii) we averaged the absolute values of the covariance for all 30 min flux periods ($n \approx 150$) between 10:00 and 16:00 PST. An example of this treatment for *m/z* 127.073 ($C_7H_{10}O_2H^+$) is shown in figure S1b within ± 30 seconds, whereas figure S1a shows the results of averaging the covariance (NOT the absolute value of the covariance) of VOC with time-shifted wind data for exactly the same set of measurements. Figure S1a indicates that the net flux (the co-variance at 0 seconds time-shift) for the one month period is very small. The value of ~ 0.005 nmol m^{-2} s^{-1} represents an upward flux (emission) but the signal is close to the noise level. From figure S1a, it is hard to argue that there is an ecosystem flux at all, because the covariance at a time-shift of 0 seconds does not emerge significantly above the noise level, a proxy of which can be considered as the variability observed between -30 and -20 or 20 and 30 second time-shifts, respectively, in figure S1a. In contrast, the sharp peak at 0 seconds in figure S2b (absolute value covariance) shows that there is an exchange with an average magnitude of 0.054 nmol m^{-2} s^{-1}. Note that information about whether the flux is up or down is lost in this representation.

As a second step, we quantified the significance of the exchange exploiting the fact that co-variance between vertical wind speed and VOC mixing ratio should be negligible when the time-shift becomes larger than the duration of the eddies that drive the transport. Therefore, for such long time-shifts, the computed covariance between the two is a measure of the noise level and can be used to determine the significance of a measured flux regardless of whether it is bi-directional or uni-directional. We considered an ion to have meaningful and detectable flux if the average daytime absolute value of the co-variance at 0 seconds (Fig. S1c) exceeds 3 times the standard deviation of two 20 second

time windows from -180 s to -160 s and from 160 s to 180 s plus the average of the two time windows. This definition is equivalent to a signal to noise ratio of 3 (S/N=3). For example, the absolute value co-variance peak for *m/z* 127.073 exceeded 4 times the standard deviation of the noise; thus S/N=4 (Fig. S1c and Table S2). From figure S1 we conclude that the ion detected at *m/z* 127.073 is both emitted and taken up by the ecosystem, though the net exchange is close to zero during daytime for the one month period of measurements.

3. Observed 24 h mean net flux, estimated 24 h mean emission, and estimated 24 h mean deposition

We calculated the 24 h mean net flux by (i) calculating the mean flux for each ion in every one hour time bin (an example diurnal trend for *m/z* 71.048, e.g. MVK+MACR is shown in figure S2b), and (ii) by averaging the 24 hourly values to a 24 h mean net flux for each ion. For estimating a 24 h mean emission (or deposition), we added up only hours with emissions (or depositions) from the diurnal trend, and then divided by 24. For example, in figure S2b there are only 2 points of depositions in the diurnal trend, so a 24 h mean deposition for MVK+MACR was estimated as the sum of these 2 deposition fluxes (at hours 5:00 and 6:00 PST) divided by 24.

4. Diurnal trend of exchange velocity (V_{ex}) for 186 ions deposited

For the 186 ions observed to have net deposition, the exchange velocity (or deposition velocity) has been evaluated according to V_{ex}= (flux) / (ambient concentration). To examine V_{ex} diurnal trends for these ions and each group, we used the median V_{ex} for each depositing ion in every one hour time bin, plotted diurnal trends for each ion, and then took the average for every hour from all depositing ions in each group. For example, every one hour data bin includes 18 median V_{ex} data from 18 ions deposited for M31-69 (Fig 3A).

5. Determination of chemical compositions

We identified the chemical formulae for 162 observed hydrocarbons and oxidized hydrocarbons with significant fluxes (Table S2). To do this, three different criteria were applied; i) absolute maximum covariance peak exceeds S/N=3, ii) exclude ions above *m/z* 237 (highly uncertain concentration estimation because they tend to have low vapor pressure, tend to be sticky, are not calibrated by standard gases, and are currently not well understood), iii) can be identified as an exact molecular formula (ion mass range within ± 3 mDa) with a combination of carbon (C), hydrogen (H), and oxygen (O) atoms using the database created by Holzinger et al. (*15*) which comprises ~18,000 possible molecular formulas. These three criteria were satisfied for 494, 353, and 162 ions, respectively. For criteria iii), alternative attributions were possible for some mass peaks to other compounds containing nitrogen (N) or sulfur (S), but we have reported compounds only as pure hydrocarbons or oxygenated hydrocarbons, thus some uncertainty in attribution remains. For example, three empirical formulae could be matched at *m/z* 175.037 within an ion mass range of ± 3 mDa, i.e. $C_{10}H_6O_3H^+$ (175.039 Da), $C_5H_6N_2O_5H^+$ (175.036 Da), and $C_6H_{10}N_2S_2H^+$ (175.035 Da). However, we assumed those masses were exclusively composed of hydrocarbons or oxidized hydrocarbons, thus $C_{10}H_6O_3H^+$ was considered as the match for *m/z* 175.037 from the example above. A total of 30 mass peaks out of 162 had similar overlaps, thus 28 mass peaks were overlapped with 2 compounds and the other 2 mass peaks with 3 compounds (Table S2).

6. Diurnal trend of 162 identified ions

Diurnal trends of the fluxes of all 162 identified ions are shown in Fig. S3a. In Figure S3b the ions have been categorized in groups of pure hydrocarbons (C_xH_y) and oxygenated VOC (OVOC) containing one, two, and three or more oxygen atoms (i.e. C_xH_yO, $C_xH_yO_2$, and $C_xH_yO_{3+}$). The fluxes shown are expressed in units of µg C m^{-2} h^{-1}. The carbon numbers were inferred from the ions detected by PTR-TOF-MS, but 10 carbons were assumed for *m/z* 81.070 and *m/z* 95.086 because these masses are known to mainly be detected due to fragmentation of monoterpenes ($C_{10}H_{16}H^+$). With the exception

of monoterpenes, we did not correct for fractionation in the drift tube of the PTR-TOF-MS. For example, para-cymene has ten carbons and only a minor fraction is detected at its protonated mass at *m/z* 135.116 ($C_{10}H_{14}H^+$); for this fraction the correct carbon number was assigned. However the main fragment detected at *m/z* 93.069 ($C_7H_8H^+$) has only 7 carbons and the carbon mass flux of this ion was calculated assuming only 7 carbons. Therefore, total carbon fluxes may be underestimated because we could not consider neutral (undetectable) fragments.

7. Leaf scale VOC emission experiment

In order to determine whether a significant number of the VOC exchanged with the citrus orchard could be attributed to leaf emissions, we measured their VOC emission directly using PTR-TOF-MS with the same measurement settings used during the field campaign. The experiment was based on our previous research by Ormeno et al. (*22*) and Fares et al. (*23*) which showed that correlations exist between terpene content and emissions from leaves of a variety of agricultural crops including citrus. Leaves were harvested in the citrus orchard and sent directly to Utrecht University, Netherlands, where the measurements were performed 6 days after harvesting. Leaves were cut into pieces, inserted into a 350 mL cuvette, which was flushed with VOC-free air at a flow of 500 standard mL min^{-1}. The cuvette with the cut leaves and an identical empty cuvette with the same flow of zero air were warmed in a water bath to 65 ^oC. An ion was considered to be observed in the head space air of the cuvette when the mixing ratios were at least three standard deviations above the background level. Three replicates were used to obtain the final results.

We found that 40% of the 162 ions to which empirical formulas were assigned (*m/z* ratios in ***bold italic*** in Table S2) were also observed as emissions from harvested leaves. Dividing these ions into 4 groups by number of oxygen, the percentages of ions observed as leaf emissions were C_xH_y – 51%, C_xH_yO – 48%, $C_xH_yO_2$ – 35%, and $C_xH_yO_{3+}$ – 24%. This result is consistent with the hypothesis that less oxygenated VOCs should be emitted from the leaves, while secondary compounds produced through atmospheric

photochemical processing should account for a larger fraction of the species containing more oxygen atoms. It should not be expected that all 162 ions exchanging with the ecosystem would be detected as emissions from harvested leaves because in the orange orchard system there are additional emission pathways that are not covered by this simple experiment: VOC observed as emission fluxes in the orchard could be due to 1) emissions of BVOC stored in the plants including the leaves, branches, flowers, fruits, and trunk, 2) emissions of BVOC produced by the plants and emitted immediately during photosynthesis or due to other plant biochemical or photochemical processes on surfaces, 3) emissions from the soil or plant litter, or 4) compounds produced by atmospheric oxidation of primary BVOC emissions. The experiments with harvested leaves specifically detect only emissions of BVOC stored in the leaves.

8. VOC reactivity with hydroxyl radicals (OH)

VOC reactivity with OH (R_{VOC}) is calculated for the following seven groups of ions: the major compounds (10 ions), C_xH_y (40 ions), C_xH_yO (30 ions), $C_xH_yO_2$ (44 ions), $C_xH_yO_{3+}$ (38 ions), other exchanging compounds (332 ions, above S/N=3), and non-exchanging compounds (61 ions, below S/N=3). Here we define R_{VOC} as:

$$R_{VOC} = \sum k_{OH+VOC} \cdot [VOC]$$

where k_{OH+VOC} is the reaction rate constant for the reaction with OH (cm^3 $molecules^{-1}$ s^{-1}) and [*VOC*] is the measured VOC concentration (molecules cm^{-3}). For the major compounds we used their known reaction rate constant with OH (values and references listed in Table S3) (*23-27*). To roughly constrain k_{OH+VOC} for the other VOC observed we selected 374 rate coefficients from the NIST chemical kinetics database (http://kinetics.nist.gov/). The selected reaction rate constants were compounds with molecular formulas that are consistent with the empirical formulas attributed to the subset of 162 ions. We calculate the 20^{th} (2.81E-12 cm^3 $molecules^{-1}$ s^{-1}), 50^{th} (1.82E-11 cm^3 $molecules^{-1}$ s^{-1}) and 80^{th} (6.37E-11 cm^3 $molecules^{-1}$ s^{-1}) percentile of the selected 374 rate coefficients and used these values as upper/lower limits and the most likely value of the

average reaction rate constant for all observed ions. The estimated R_{VOC} for the lower limit, best estimate, and upper limit for the reaction rate constant is 5.13 s^{-1}, 11.76 s^{-1}, and 31.39 s^{-1}, respectively (Table 3). These values are within the range of reported total OH reactivity measurement above different ecosystems (*28*). The contribution of each group to R_{VOC} is shown in Figure S4 for the best estimate of the reaction rate constant. While this estimate is necessarily crude due to lack of specific VOC chemical identifications and their reactions rates with OH, it demonstrates the potential importance of the observed ions in terms of contributions to regional photochemistry. The major compounds represented by 10 ions contribute 33% to the total estimated reactivity of 11.8 s^{-1} from all 555 observed ions, whereas the 484 minor ions that exchange with the ecosystem are estimated to contribute 62% to the total reactivity.

9. Possible global importance for secondary organic aerosol formation

Many of the observed minor ions contain sufficient carbon atoms and oxygen functional groups to likely partition into the condensed phase or contribute to new particle formation. Dry deposition of these compounds is in direct competition with formation of SOA. Therefore it is of great importance to measure deposition rates in other globally relevant ecosystems, particularly those in regions with higher BVOC emission rates. If the estimated deposition (Fig 2D) holds for a total land vegetation surface area of 50 million km^2, the total sink is calculated at 270 Tg C per year, which is the upper limit for the global VOC sink due to wet and dry deposition as estimated by Goldstein and Galbally (5), but still lower than the deposition estimated by Hallquist et al. (10). Similar back of the envelope calculations demonstrate the potential global importance of the emission of these minor compounds.

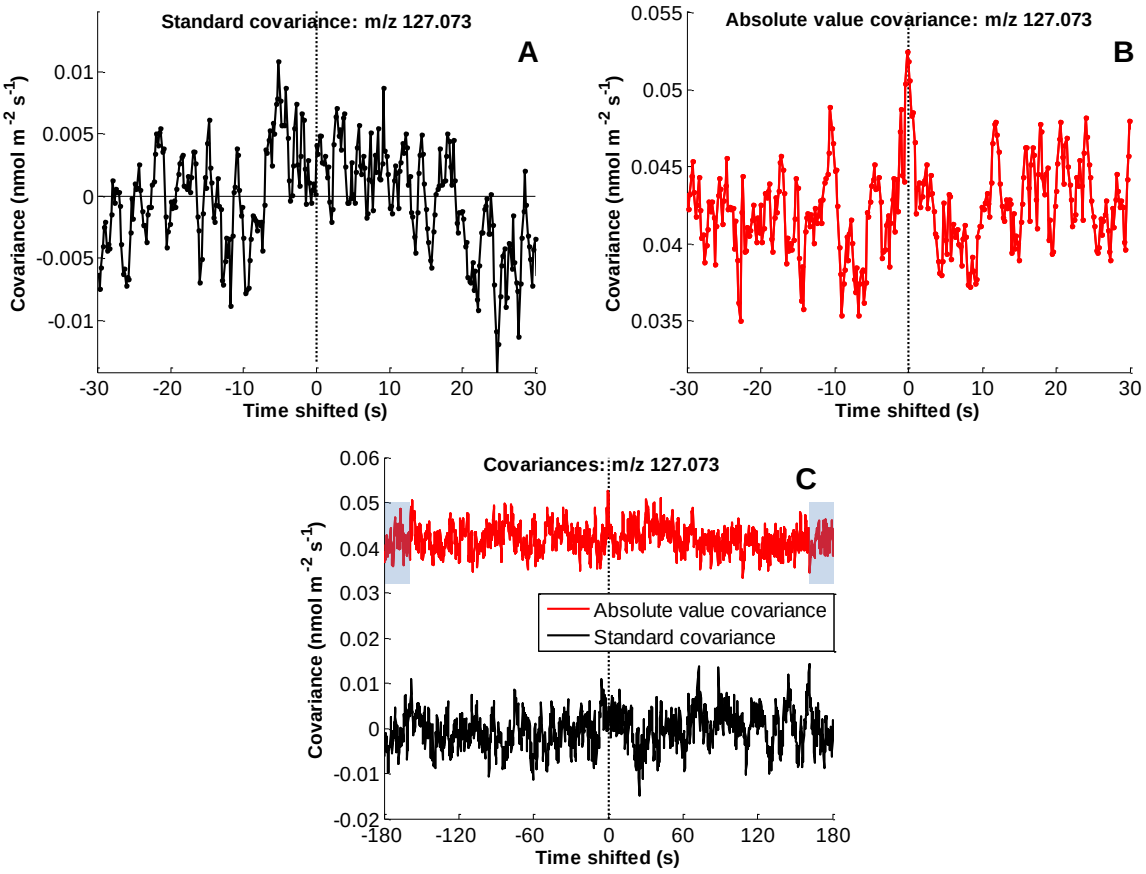

Fig. S1. Time-shifted covariance plots of vertical wind speed and *m/z* 127.073 ($C_7H_{10}O_2H^+$) observed by PTR-TOF-MS, averaged over 10:00 – 16:00 PST throughout the whole measurement campaign with (A) standard co-variance analysis in ± 30 s time window, (B) absolute value co-variance analysis ± 30 s, and (C) both analyses (standard co-variance in black line and absolute value co-variance in red line) in ± 180 s for each 30 min data period. The standard deviation of the data in the shaded area in C is assumed to represent the noise of the signal for absolute value co-variance analysis. A sharp peak at 0 s in B and C (red line) indicates apparent exchange for *m/z* 127.073, which is not observed in A and C (black line) due to bi-directional exchange masking the flux.

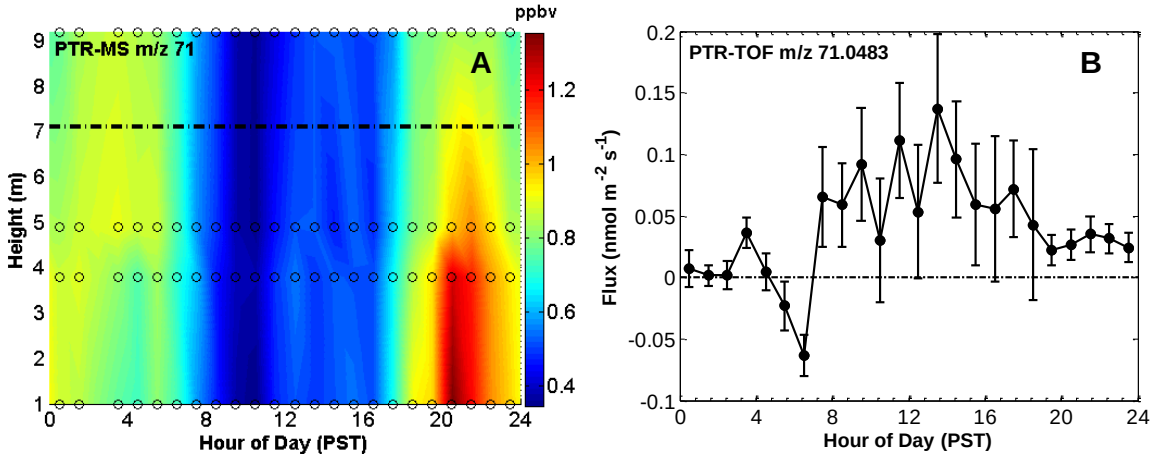

Fig. S2. Mean vertical gradient measured by PTR-MS (A) and flux measured by PTR-TOF-MS (B) of the diurnal pattern for the sum of methylvinylketone and methacrolein (MVK+MACR) (Park et al., 2012). Interpolated gradient measurements (A) are color coded with actual measurement timing and vertical positions shown as open circles, and flux measurement height shown as a broken black line. Flux diurnal patterns of MVK+MACR shown in B agree well with observed vertical gradients during day and night with net emission. Error bars in B denote the standard deviations of all measurements at the respective hour of the day.

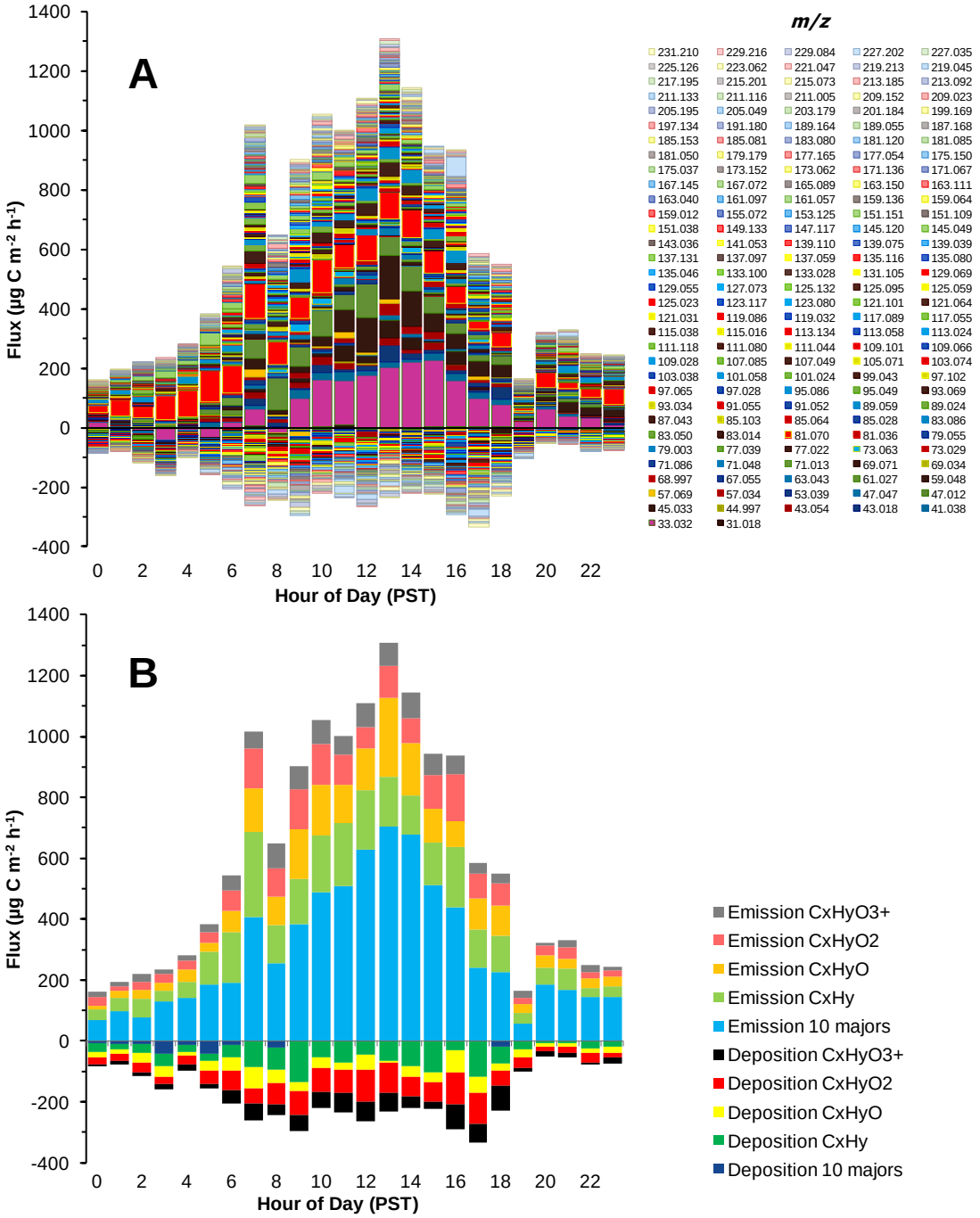

Fig. S3. Total VOC diurnal flux measured by PTR-TOF-MS on a carbon mass basis. Staged bar plots of 162 ions with *m/z* indicated in the legend (A), and 4 hydrocarbon groups classified by the number of oxygen and as fifth group the 10 major dominant compounds at the site (B).

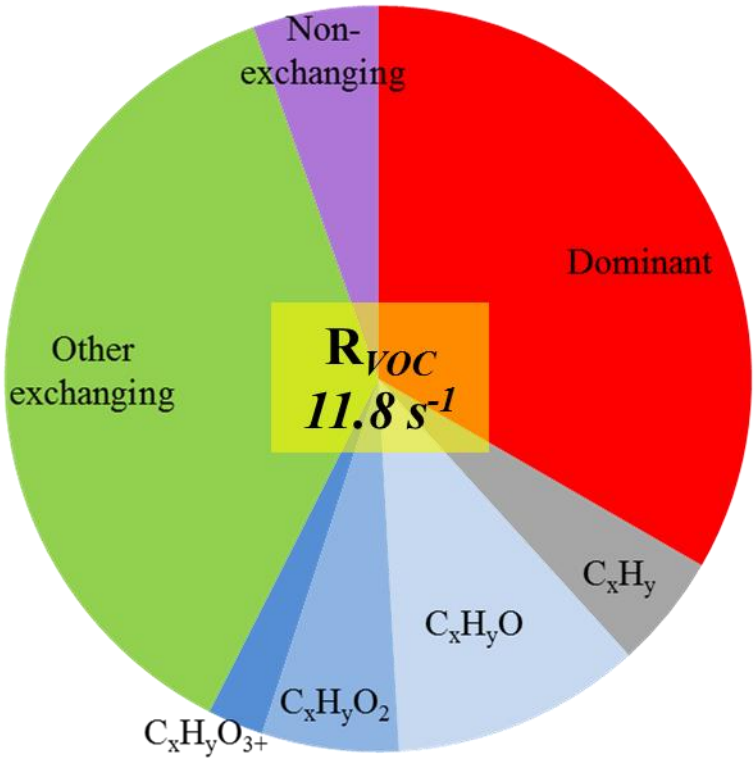

Fig. S4. VOC reactivity with OH (R_{VOC}) estimated for the 555 observed ions. R_{VOC} contributions are categorized by groups according to our knowledge of their chemical formulae and whether they actively exchange at the ecosystem-atmosphere interface: dominant compounds (10 ions, 33% of total R_{VOC}), C_xH_y (40 ions, 5%), C_xH_yO (30 ions, 11%), $C_xH_yO_2$ (44 ions, 6%), $C_xH_yO_{3+}$ (38 ions, 3%), other exchanging compounds (332 ions, 37%), non-exchanging compounds (61 ions, 5%).

Table S1. Summarized flux for the 10 major ions including monoterpenes (*m/z* 81.070 + 137.131 + 95.086), methanol (*m/z* 33.032), acetone (*m/z* 59.048), acetic acid (*m/z* 61.027), para-cymene (*m/z* 93.069), acetaldehyde (*m/z* 45.033), MVK+MACR (*m/z* 71.048), and isoprene+MBO (*m/z* 69.071) and 4 groups of ions summed as *m/z* ranges 31-69 (M31-69), 69-136 (M69-136), 136-237 (M136-237), and 237-1278 (M237-1278). Data are separated into fluxes on a molar and carbon mass basis (left four columns) and flux and exchange velocity (V_{ex}) by 4 groups for the 186 ions which showed a 24 h net deposition flux (right 3 columns).

		Molar basis	Carbon mass basis	Depositing ions		
Group	# of ions	Net flux 24 h mean [nmol m^{-2} s^{-1}] (24 h mean emission /deposition)	Net flux 24 h mean [µg C m^{-2} h^{-1}] (24 h mean emission /deposition)	# of ions	Net flux 24 h mean [nmol m^{-2} s^{-1}] (24 h mean emission /deposition)	24h mean V_{ex} [cm s^{-1}]
10 majors	10	2.82 (2.95 / -0.13)	287 (294 / -7.7)	0		
M31-69	61	1.09 (2.97 / -1.88)	94 (257 / -163)	18	-0.27 (0.39 / -0.66)	-0.19
M69-136	141	0.45 (1.06 / -0.61)	96 (229 / -132)	40	-0.07 (0.18 / -0.24)	-0.24
M136-237	141	0.06 (0.42 / -0.37)	24 (183 / -158)	57	-0.07 (0.12 / -0.19)	-0.41
M237-1278	141	0.02 (0.27 / -0.25)	11 (174 / -163)	71	-0.05 (0.1 / -0.15)	-0.32

Table S2. Mixing ratio and eddy covariance flux measured for 162 ions to which an empirical formula has been attributed.

Mass to charge observed (m/z) [a]	Possible empirical formulae	Δ mDa [b]	Mixing ratio [nmol mol^{-1}] 24 h mean (day/night)	EC flux [µg C m^{-2} h^{-1}] 24 h mean net flux (24 h mean emission/deposition)	S/N criterion
31.018	CH_2OH^+	-0.16	0.36 (0.31 / 0.41)	0.86 (1.76 / -0.9)	5
33.032	CH_4OH^+	1.39	19.89 (16.85 / 24.55)	71.5 (75.9 / -4.39)	10
41.038	$C_3H_4H^+$	0.28	0.39 (0.2 / 0.51)	10.96 (11.58 / -0.62)	3
43.018	$C_2H_2OH^+$	-0.16	1.03 (0.96 / 1.25)	10.92 (11.49 / -0.58)	5
43.054	$C_3H_6H^+$	0.23	0.37 (0.27 / 0.46)	9.7 (9.86 / -0.16)	7
44.997	CO_2H^+	-0.09	0.19 (0.14 / 0.23)	-0.78 (0.9 / -1.68)	3
45.033	$C_2H_4OH^+$	0.89	2.92 (2.77 / 3.18)	11.46 (12.82 / -1.36)	8
47.012	$CH_2O_2H^+$	0.86	0.17 (0.19 / 0.16)	-1.12 (0.35 / -1.47)	5
47.047	$C_2H_6OH^+$	2.34	0.77 (0.65 / 0.93)	1.67 (2.93 / -1.26)	4
53.039	$C_4H_4H^+$	-0.22	0.08 (0.07 / 0.1)	2.13 (3.66 / -1.54)	4
57.034	$C_3H_4OH^+$	-0.61	0.28 (0.2 / 0.36)	4.33 (6.36 / -2.03)	3
57.069	$C_4H_8H^+$	0.48	0.11 (0.07 / 0.14)	2.81 (4.66 / -1.85)	7
59.048	$C_3H_6OH^+$	0.94	4.52 (3.73 / 5.35)	36.48 (37.02 / -0.54)	10
61.027	$C_2H_4O_2H^+$	1.21	4.9 (5.05 / 5.47)	35.68 (36.11 / -0.43)	8
63.043	$C_2H_6O_2H^+$	1.26	0.061 (0.058 / 0.067)	-0.17 (0.57 / -0.75)	3
67.055	$C_5H_6H^+$	-0.67	0.058 (0.03 / 0.081)	2.64 (3.6 / -0.95)	4
68.997	$C_3O_2H^+$	0.41	0.037 (0.036 / 0.038)	0.62 (0.93 / -0.31)	5
69.034	$C_4H_4OH^+$	-0.61	0.052 (0.038 / 0.063)	0.26 (1.33 / -1.07)	6
69.071	$C_5H_8H^+$	-0.82	0.28 (0.19 / 0.34)	5.31 (5.45 / -0.14)	8
71.013	$C_3H_2O_2H^+$	-0.34	0.04 (0.04 / 0.05)	0.43 (1.23 / -0.8)	5
71.048	$C_4H_6OH^+$	0.84	0.3 (0.2 / 0.36)	7.05 (7.67 / -0.62)	8
71.086	$C_5H_{10}H^+$	-0.27	0.049 (0.032 / 0.06)	1.33 (2.39 / -1.05)	5
73.029	$C_3H_4O_2H^+$	-0.69	0.2 (0.15 / 0.15)	-0.23 (1.67 / -1.9)	4
73.063	$C_4H_8OH^+$	2.19	0.38 (0.3 / 0.45)	5 (6.17 / -1.18)	3
77.022	$C_2H_4O_3H^+$	1.52	0.044 (0.038 / 0.052)	0.83 (1.39 / -0.55)	5
77.039	$C_6H_4H^+$ $C_3H_8SH^+$	-0.52 2.85	0.08 (0.05 / 0.12)	4.89 (6.05 / -1.15)	4
79.003	$CH_2O_4H^+$	-0.11	0.026 (0.025 / 0.028)	0.04 (0.29 / -0.25)	3
79.055	$C_6H_6H^+$	-0.37	0.1 (0.06 / 0.14)	4.14 (4.65 / -0.51)	4
81.036	$C_5H_4OH^+$	-2.01	0.05 (0.027 / 0.068)	3.19 (3.42 / -0.23)	4
81.070	$C_6H_8H^+$	-0.12	0.5 (0.23 / 0.73)	65.62 (65.62 / 0)	10
83.014	$C_4H_2O_2H^+$	-0.74	0.032 (0.027 / 0.035)	0.09 (0.85 / -0.76)	3
83.050	$C_5H_6OH^+$	-0.86	0.09 (0.03 / 0.14)	1.84 (2.62 / -0.78)	4
83.086	$C_6H_{10}H^+$	-0.57	0.13 (0.08 / 0.16)	1.72 (2.79 / -1.07)	4

85.028	$C_4H_4O_2H^+$	0.21	0.08 (0.06 / 0.1)	0.52 (1.53 / -1.01)	3
85.064	$C_5H_8OH^+$	0.89	0.07 (0.03 / 0.1)	1.71 (2.76 / -1.06)	4
85.103	$C_6H_{12}H^+$	-1.32	0.027 (0.019 / 0.032)	0.44 (1.86 / -1.42)	3
87.043	$C_4H_6O_2H^+$	1.26	0.22 (0.16 / 0.28)	2.46 (3.38 / -0.92)	6
89.024	$C_3H_4O_3H^+$	-0.48	0.04 (0.04 / 0.04)	0.9 (1.37 / -0.47)	5
89.059	$C_4H_8O_2H^+$	1.21	0.09 (0.08 / 0.1)	0.55 (1.81 / -1.26)	4
91.052	$C_7H_6H^+$	2.63	0.037 (0.017 / 0.054)	2.28 (2.76 / -0.48)	3
	$C_2H_6N_2O_2H^+$	-1.40			
91.055	$C_7H_6H^+$	-0.67	0.057 (0.021 / 0.088)	1.93 (3.06 / -1.13)	5
	$C_4H_{10}SH^+$	2.70			
93.034	$C_6H_4OH^+$	-0.11	0.056 (0.042 / 0.071)	4.17 (5.19 / -1.02)	4
93.069	$C_7H_8H^+$	0.78	0.14 (0.04 / 0.22)	17.41 (17.41 / 0)	8
95.049	$C_6H_6OH^+$	0.54	0.056 (0.032 / 0.074)	4.47 (4.81 / -0.34)	4
95.086	$C_7H_{10}H^+$	-0.47	0.25 (0.17 / 0.32)	20.11 (20.3 / -0.19)	9
97.028	$C_5H_4O_2H^+$	0.11	0.061 (0.032 / 0.086)	1.47 (2.53 / -1.06)	4
97.065	$C_6H_8OH^+$	-0.21	0.07 (0.02 / 0.1)	1.29 (2.56 / -1.26)	4
97.102	$C_7H_{12}H^+$	-0.42	0.038 (0.017 / 0.054)	0.93 (2.03 / -1.11)	3
99.043	$C_5H_6O_2H^+$	0.66	0.08 (0.04 / 0.12)	1.74 (2.57 / -0.84)	4
101.024	$C_4H_4O_3H^+$	-0.68	0.041 (0.035 / 0.047)	1.64 (2.24 / -0.6)	7
101.058	$C_5H_8O_2H^+$	1.71	0.08 (0.04 / 0.11)	0.88 (1.63 / -0.74)	5
103.038	$C_4H_6O_3H^+$	0.97	0.036 (0.033 / 0.038)	0.15 (1.02 / -0.87)	5
103.074	$C_5H_{10}O_2H^+$	1.36	0.042 (0.033 / 0.041)	1.4 (2.18 / -0.78)	5
105.071	$C_8H_8H^+$	-1.12	0.055 (0.019 / 0.085)	1.14 (2.67 / -1.53)	5
	$C_5H_{12}SH^+$	2.25			
107.049	$C_7H_6OH^+$	0.14	0.053 (0.012 / 0.087)	1.65 (2.49 / -0.84)	4
107.085	$C_8H_{10}H^+$	0.53	0.08 (0.01 / 0.12)	5.6 (6.19 / -0.59)	4
109.028	$C_6H_4O_2H^+$	0.41	0.025 (0.022 / 0.027)	0.79 (1.72 / -0.93)	3
109.066	$C_7H_8OH^+$	-1.21	0.034 (0.015 / 0.046)	0.45 (1.47 / -1.02)	6
109.101	$C_8H_{12}H^+$	0.18	0.033 (0.011 / 0.049)	0.31 (1.95 / -1.64)	5
111.044	$C_6H_6O_2H^+$	0.06	0.037 (0.021 / 0.048)	1.19 (1.87 / -0.68)	5
111.080	$C_7H_{10}OH^+$	0.44	0.056 (0.033 / 0.071)	0.72 (1.67 / -0.95)	3
111.118	$C_8H_{14}H^+$	-1.17	0.031 (0.023 / 0.037)	-1.24 (0.89 / -2.13)	3
113.024	$C_5H_4O_3H^+$	-0.68	0.064 (0.063 / 0.064)	-0.01 (1.48 / -1.49)	4
113.058	$C_6H_8O_2H^+$	1.71	0.049 (0.03 / 0.061)	-0.19 (1.2 / -1.39)	5
113.134	$C_8H_{16}H^+$	-1.52	0.017 (0.015 / 0.019)	-0.16 (0.93 / -1.09)	7
115.016	$C_8H_2OH^+$	1.84	0.03 (0.03 / 0.03)	-0.09 (1.37 / -1.46)	5
	$C_3H_2N_2O_3H^+$	-2.18			
115.038	$C_5H_6O_3H^+$	0.97	0.034 (0.029 / 0.038)	0.19 (0.87 / -0.67)	4
117.055	$C_5H_8O_3H^+$	-0.38	0.02 (0.018 / 0.021)	0.01 (0.65 / -0.64)	3
117.089	$C_6H_{12}O_2H^+$	2.01	0.034 (0.024 / 0.033)	0.51 (1.62 / -1.11)	5
119.032	$C_4H_6O_4H^+$	1.89	0.014 (0.012 / 0.015)	0.91 (1.11 / -0.2)	3
119.086	$C_9H_{10}H^+$	-0.47	0.041 (0.024 / 0.05)	-0.16 (1.96 / -2.11)	4
	$C_6H_{14}SH^+$	2.90			

121.031	$C_7H_4O_2H^+$	-2.59	0.031 (0.016 / 0.046)	0.32 (1.51 / -1.2)	3
	$C_4H_8O_2SH^+$	0.78			
121.064	$C_8H_8OH^+$	0.79	0.031 (0.014 / 0.045)	0.99 (1.73 / -0.74)	5
121.101	$C_9H_{12}H^+$	0.18	0.072 (0.023 / 0.112)	2.54 (3.34 / -0.8)	4
123.080	$C_8H_{10}OH^+$	0.44	0.026 (0.017 / 0.033)	0.88 (1.68 / -0.8)	4
123.117	$C_9H_{14}H^+$	-0.17	0.019 (0.008 / 0.027)	2.34 (2.74 / -0.4)	3
125.023	$C_6H_4O_3H^+$	0.32	0.023 (0.019 / 0.026)	1.1 (1.71 / -0.61)	3
125.059	$C_7H_8O_2H^+$	0.71	0.017 (0.009 / 0.023)	0.89 (1.38 / -0.49)	4
125.095	$C_8H_{12}OH^+$	1.09	0.022 (0.01 / 0.03)	0.39 (2.08 / -1.7)	4
125.132	$C_9H_{16}H^+$	0.48	0.019 (0.015 / 0.022)	-0.28 (1.69 / -1.97)	3
127.073	$C_7H_{10}O_2H^+$	2.36	0.03 (0.02 / 0.038)	1.6 (2.13 / -0.54)	4
129.055	$C_6H_8O_3H^+$	-0.38	0.015 (0.012 / 0.017)	0.35 (0.94 / -0.59)	5
129.069	$C_{10}H_8H^+$	0.88	0.029 (0.018 / 0.033)	0.24 (1.68 / -1.44)	4
131.105	$C_7H_{14}O_2H^+$	1.66	0.017 (0.014 / 0.019)	1.51 (2.18 / -0.67)	4
133.028	$C_8H_4O_2H^+$	0.41	0.013 (0.011 / 0.014)	0.22 (1.37 / -1.15)	6
133.100	$C_{10}H_{12}H^+$	1.18	0.046 (0.021 / 0.065)	4.13 (4.29 / -0.16)	5
	$C_5H_{12}N_2O_2H^+$	-2.85			
135.046	$C_8H_6O_2H^+$	-1.94	0.015 (0.009 / 0.02)	0.82 (1.44 / -0.62)	3
	$C_5H_{10}O_2SH^+$	1.43			
135.080	$C_9H_{10}OH^+$	0.44	0.041 (0.023 / 0.048)	1.29 (1.91 / -0.62)	3
135.116	$C_{10}H_{14}H^+$	0.83	0.094 (0.055 / 0.102)	2.28 (3.12 / -0.83)	6
137.059	$C_8H_8O_2H^+$	-0.64	0.017 (0.011 / 0.021)	0.46 (1.15 / -0.69)	4
137.097	$C_9H_{12}OH^+$	-0.91	0.034 (0.015 / 0.049)	3.23 (3.54 / -0.32)	4
137.131	$C_{10}H_{16}H^+$	1.48	0.12 (0.05 / 0.18)	15.94 (15.94 / 0)	10
139.039	$C_7H_6O_3H^+$	-0.03	0.021 (0.015 / 0.025)	0.75 (1.51 / -0.76)	5
139.075	$C_8H_{10}O_2H^+$	0.36	0.023 (0.013 / 0.031)	0.9 (1.59 / -0.7)	5
139.110	$C_9H_{14}OH^+$	1.74	0.032 (0.005 / 0.051)	-0.15 (1.64 / -1.78)	4
141.053	$C_7H_8O_3H^+$	1.62	0.019 (0.015 / 0.02)	0.94 (1.57 / -0.63)	6
	$C_2H_8N_2O_5H^+$	-2.40			
143.036	$C_6H_6O_4H^+$	-2.11	0.019 (0.018 / 0.021)	0.55 (1.04 / -0.49)	3
145.049	$C_6H_8O_4H^+$	0.54	0.011 (0.01 / 0.013)	-0.47 (0.5 / -0.97)	4
145.120	$C_8H_{16}O_2H^+$	2.31	0.015 (0.014 / 0.016)	0.01 (1.1 / -1.09)	6
147.117	$C_{11}H_{14}H^+$	-0.17	0.015 (0.012 / 0.016)	-0.94 (1.22 / -2.16)	4
149.133	$C_{11}H_{16}H^+$	-0.52	0.015 (0.008 / 0.02)	0.7 (1.61 / -0.91)	3
151.038	$C_8H_6O_3H^+$	0.97	0.019 (0.015 / 0.022)	-0.04 (1.39 / -1.43)	5
	$C_4H_{10}N_2S_2H^+$	-2.19			
151.109	$C_{10}H_{14}OH^+$	2.74	0.018 (0.008 / 0.024)	1.04 (2.36 / -1.32)	6
	$C_5H_{14}N_2O_3H^+$	-1.28			
151.151	$C_{11}H_{18}H^+$	-2.87	0.013 (0.01 / 0.015)	1.02 (1.64 / -0.62)	4
153.125	$C_{10}H_{16}OH^+$	2.39	0.025 (0.012 / 0.035)	1.36 (2.62 / -1.27)	3
155.072	$C_8H_{10}O_3H^+$	-1.73	0.014 (0.014 / 0.014)	0.57 (1.19 / -0.62)	4
159.012	$C_2H_6O_8H^+$	1.55	0.012 (0.012 / 0.011)	-0.06 (0.14 / -0.2)	4
	$C_6H_6O_3SH^+$	-0.96			
159.064	$C_7H_{10}O_4H^+$	1.19	0.016 (0.015 / 0.016)	0.52 (1.09 / -0.57)	5

159.136	$C_9H_{18}O_2H^+$	1.96	0.012 (0.011 / 0.014)	0.75 (1.71 / -0.97)	4
161.057	$C_{10}H_8O_2H^+$	2.71	0.017 (0.016 / 0.018)	0.14 (1.15 / -1.01)	4
	$C_5H_8N_2O_4H^+$	-1.32			
161.097	$C_{11}H_{12}OH^+$	-0.91	0.013 (0.012 / 0.015)	0.1 (1.52 / -1.42)	3
	$C_8H_{16}OSH^+$	2.46			
163.040	$C_9H_6O_3H^+$	-1.03	0.015 (0.013 / 0.016)	-0.68 (0.76 / -1.44)	4
163.111	$C_{11}H_{14}OH^+$	0.74	0.011 (0.009 / 0.012)	1.66 (2.27 / -0.62)	5
163.150	$C_{12}H_{18}H^+$	-1.87	0.011 (0.009 / 0.013)	0.57 (1.7 / -1.13)	3
165.089	$C_{10}H_{12}O_2H^+$	2.01	0.015 (0.01 / 0.018)	0.63 (1.83 / -1.2)	5
	$C_5H_{12}N_2O_4H^+$	-2.02			
167.072	$C_9H_{10}O_3H^+$	-1.73	0.009 (0.007 / 0.01)	0.75 (1.38 / -0.63)	4
	$C_6H_{14}O_3SH^+$	1.64			
167.145	$C_{11}H_{18}OH^+$	-1.96	0.015 (0.013 / 0.016)	0.73 (1.73 / -1)	4
171.067	$C_8H_{10}O_4H^+$	-1.81	0.01 (0.009 / 0.011)	0.48 (1.01 / -0.53)	3
171.136	$C_{10}H_{18}O_2H^+$	1.96	0.016 (0.014 / 0.017)	-0.27 (1.02 / -1.29)	4
173.062	$C_{11}H_8O_2H^+$	-2.29	0.015 (0.014 / 0.015)	-0.87 (0.58 / -1.45)	3
173.152	$C_{10}H_{20}O_2H^+$	1.61	0.014 (0.013 / 0.015)	0.48 (1.52 / -1.04)	4
175.037	$C_{10}H_6O_3H^+$	1.97	0.015 (0.014 / 0.015)	0.13 (1.29 / -1.16)	3
	$C_5H_6N_2O_5H^+$	-2.05			
	$C_6H_{10}N_2S_2H^+$	-1.19			
175.150	$C_{13}H_{18}H^+$	-1.87	0.012 (0.011 / 0.013)	-0.24 (1.43 / -1.67)	3
	$C_{10}H_{22}SH^+$	1.50			
177.054	$C_{10}H_8O_3H^+$	0.62	0.015 (0.015 / 0.016)	0.41 (1.85 / -1.45)	4
	$C_6H_{12}N_2S_2H^+$	-2.54			
177.165	$C_{13}H_{20}H^+$	-1.22	0.014 (0.012 / 0.015)	1.14 (2.44 / -1.3)	6
179.179	$C_{13}H_{22}H^+$	0.43	0.01 (0.009 / 0.011)	0.37 (1.79 / -1.42)	4
181.050	$C_9H_8O_4H^+$	-0.46	0.009 (0.009 / 0.01)	-0.67 (0.53 / -1.2)	5
181.085	$C_{10}H_{12}O_3H^+$	0.92	0.007 (0.006 / 0.008)	-0.43 (0.58 / -1.01)	4
181.120	$C_{11}H_{16}O_2H^+$	2.31	0.01 (0.008 / 0.011)	0.33 (1.49 / -1.16)	3
	$C_6H_{16}N_2O_4H^+$	-1.72			
183.080	$C_{13}H_{10}OH^+$	0.44	0.011 (0.009 / 0.012)	1.29 (2.01 / -0.72)	4
185.081	$C_9H_{12}O_4H^+$	-0.16	0.01 (0.01 / 0.011)	0.09 (0.79 / -0.7)	3
185.153	$C_{11}H_{20}O_2H^+$	0.61	0.012 (0.011 / 0.012)	0.32 (1.64 / -1.33)	3
187.168	$C_{11}H_{22}O_2H^+$	1.26	0.01 (0.009 / 0.011)	-1.66 (0.66 / -2.33)	6
189.055	$C_{11}H_8O_3H^+$	-0.38	0.012 (0.012 / 0.012)	0.32 (1.25 / -0.93)	4
189.164	$C_{14}H_{20}H^+$	-0.22	0.012 (0.011 / 0.013)	0.62 (1.38 / -0.76)	4
191.180	$C_{14}H_{22}H^+$	-0.57	0.013 (0.012 / 0.014)	0.03 (1.67 / -1.65)	5
197.134	$C_{15}H_{16}H^+$	-1.52	0.014 (0.013 / 0.014)	0.02 (1.4 / -1.38)	4
	$C_{12}H_{20}SH^+$	1.85			
199.169	$C_{12}H_{22}O_2H^+$	0.26	0.01 (0.01 / 0.011)	0.08 (1.27 / -1.2)	4
201.184	$C_{12}H_{24}O_2H^+$	0.91	0.013 (0.011 / 0.015)	-0.8 (1.2 / -2)	4
203.179	$C_{15}H_{22}H^+$	0.43	0.01 (0.009 / 0.011)	-1.6 (1.15 / -2.75)	4
205.049	$C_{11}H_8O_4H^+$	0.54	0.006 (0.006 / 0.007)	-1.03 (0.41 / -1.44)	4
205.195	$C_{15}H_{24}H^+$	0.08	0.02 (0.017 / 0.023)	0.8 (1.93 / -1.14)	4
209.023	$C_{13}H_4O_3H^+$	0.32	0.011 (0.01 / 0.012)	0 (1.87 / -1.87)	3

	$C_5H_8N_2O_5SH^+$	-0.33			
209.152	$C_{13}H_{20}O_2H^+$	1.61	0.013 (0.013 / 0.014)	0.31 (1.32 / -1.02)	3
	$C_8H_{20}N_2O_4H^+$	-2.42			
211.005	$C_{12}H_2O_4H^+$	-2.41	0.018 (0.018 / 0.018)	0.08 (1.28 / -1.2)	5
	$C_9H_6O_4SH^+$	0.96			
211.116	$C_8H_{18}O_6H^+$	1.62	0.007 (0.007 / 0.007)	0.09 (0.85 / -0.76)	4
	$C_{12}H_{18}OSH^+$	-0.89			
211.133	$C_{12}H_{18}O_3H^+$	-0.13	0.01 (0.009 / 0.01)	-1.01 (0.54 / -1.55)	5
213.092	$C_{14}H_{12}O_2H^+$	-0.99	0.009 (0.009 / 0.009)	-0.46 (0.81 / -1.27)	6
213.185	$C_{13}H_{24}O_2H^+$	-0.09	0.009 (0.009 / 0.01)	1.37 (2.12 / -0.74)	6
215.073	$C_{13}H_{10}O_3H^+$	-2.73	0.01 (0.01 / 0.01)	-0.69 (1.17 / -1.86)	5
	$C_{10}H_{14}O_3SH^+$	0.64			
215.201	$C_{13}H_{26}O_2H^+$	-0.44	0.009 (0.008 / 0.009)	-0.38 (0.93 / -1.31)	4
217.195	$C_{16}H_{24}H^+$	0.08	0.009 (0.009 / 0.01)	-0.94 (1.04 / -1.98)	6
219.045	$C_{15}H_6O_2H^+$	-0.94	0.13 (0.13 / 0.1)	-1.26 (4.83 / -6.09)	4
	$C_{12}H_{10}O_2SH^+$	2.43			
219.213	$C_{16}H_{26}H^+$	-2.27	0.011 (0.01 / 0.012)	-0.71 (1.86 / -2.56)	3
221.047	$C_{11}H_8O_5H^+$	-2.55	0.018 (0.019 / 0.016)	0.36 (1.49 / -1.13)	4
223.062	$C_{11}H_{10}O_5H^+$	-1.90	0.023 (0.02 / 0.028)	-1.6 (1.2 / -2.8)	5
225.126	$C_{16}H_{16}OH^+$	1.39	0.012 (0.011 / 0.013)	-1.45 (0.47 / -1.92)	3
	$C_{11}H_{16}N_2O_3H^+$	-2.63			
227.035	$C_{13}H_6O_4H^+$	-1.11	0.008 (0.008 / 0.008)	1.74 (2.54 / -0.8)	3
227.202	$C_{14}H_{26}O_2H^+$	-1.44	0.009 (0.009 / 0.01)	-2.31 (0.59 / -2.9)	3
229.084	$C_{14}H_{12}O_3H^+$	1.92	0.012 (0.01 / 0.014)	0.26 (1.36 / -1.11)	3
	$C_9H_{12}N_2O_5H^+$	-2.10			
	$C_{10}H_{16}N_2S_2H^+$	-1.24			
229.216	$C_{14}H_{28}O_2H^+$	0.21	0.011 (0.009 / 0.015)	0.91 (1.94 / -1.02)	3
231.210	$C_{17}H_{26}H^+$	0.73	0.011 (0.01 / 0.011)	0.33 (1.58 / -1.25)	4

[a] Mass to charge ratio (m/z) values highlighted in ***bold italic*** were also observed in emissions from harvested leaves.

[b] The difference between the exact ion mass and the measured mass in mDa.

Table S3. The estimated 20th, 50th, and 80th percentile VOC reactivity with OH for 7 VOC groups observed.

m/z	Chemical assumed	k_{OH+VOC} (cm^3 $molec^{-1}$ s^{-1})		References	R_{VOC} (s^{-1})
33.0321	Methanol	9.28E-13		Atkinson et al. (*24*)	0.38
45.0326	Acetaldehyde	1.62E-11		Atkinson (*25*)	1.09
59.0482	Acetone	2.19E-13		Atkinson et al. (*24*)	0.02
61.0272	Acetic acid	8E-13		Atkinson et al. (*24*)	0.10
69.0707	Isoprene	1E-10		Atkinson (*25*)	0.46
71.0483	50% MVK + 50% MACR	1.85E-11 3.07E-11		Atkinson (*25*)	0.12
81.0700	Limonene	1.61E-10		Gill and Hites (*26*)	0.88
93.0691	Para-cymene	1.51E-11		Corchnoy and Atkinson (*27*)	0.02
95.0860	Limonene	1.61E-10		Gill and Hites (*26*)	0.65
137.131	Limonene	1.61E-10		Gill and Hites (*26*)	0.21
	10 dominant compounds			Subtotal	3.92
31-231	C_xH_y (40 ions)	2.81E-12	20th	NIST kinetics database	0.09
		1.82E-11	50th		0.58
		6.37E-11	80th		2.04
31-231	C_xH_yO (30 ions)	2.81E-12	20th	NIST kinetics database	0.20
		1.82E-11	50th		1.27
		6.37E-11	80th		4.46
31-231	$C_xH_yO_2$ (44 ions)	2.81E-12	20th	NIST kinetics database	0.11
		1.82E-11	50th		0.70
		6.37E-11	80th		2.44
31-231	$C_xH_yO_3$ (38 ions)	2.81E-12	20th	NIST kinetics database	0.04
		1.82E-11	50th		0.29
		6.37E-11	80th		1.00
31-1263	Other Exchanging compounds (309 ions)	2.81E-12	20th	NIST kinetics database	0.67
		1.82E-11	50th		4.36
		6.37E-11	80th		15.3
31-1263	Non-exchanging Compounds (61 ions)	2.81E-12	20th	NIST kinetics database	0.10
		1.82E-11	50th		0.64
		6.37E-11	80th		2.23
	All 555 ions observed		20th	Sum	5.13
			50th		11.8
			80th		31.4

References and Notes

1. A. Guenther, C. N. Hewitt, D. Erickson, R. Fall, C. Geron, T. Graedel, P. Harley, L. Klinger, M. Lerdau, W. A. Mckay, T. Pierce, B. Scholes, R. Steinbrecher, R. Tallamraju, J. Taylor, P. Zimmerman, A global-model of natural volatile organic-compound emissions. *J. Geophys. Res. Atmos.* **100**, 8873 (1995). doi:10.1029/94JD02950

2. W. L. Chameides, R. W. Lindsay, J. Richardson, C. S. Kiang, The role of biogenic hydrocarbons in urban photochemical smog: Atlanta as a case study. *Science* **241**, 1473–1475 (1988). doi:10.1126/science.3420404 Medline

3. M. O. Andreae, P. J. Crutzen, Atmospheric aerosols: Biogeochemical sources and role in atmospheric chemistry. *Science* **276**, 1052–1058 (1997). doi:10.1126/science.276.5315.1052

4. M. S. Jang, N. M. Czoschke, S. Lee, R. M. Kamens, Heterogeneous atmospheric aerosol production by acid-catalyzed particle-phase reactions. *Science* **298**, 814–817 (2002). doi:10.1126/science.1075798 Medline

5. A. H. Goldstein, I. E. Galbally, Known and unexplored organic constituents in the Earth' s atmosphere. *Environ. Sci. Technol.* **41**, 1514–1521 (2007). doi:10.1021/es072476p Medline

6. M. R. Kurpius, A. H. Goldstein, Gas-phase chemistry dominates O_3 loss to a forest, implying a source of aerosols and hydroxyl radicals to the atmosphere. *Geophys. Res. Lett.* **30**, 1371 (2003). doi:10.1029/2002GL016785

7. P. Di Carlo, W. H. Brune, M. Martinez, H. Harder, R. Lesher, X. Ren, T. Thornberry, M. A. Carroll, V. Young, P. B. Shepson, D. Riemer, E. Apel, C. Campbell, Missing OH reactivity in a forest: Evidence for unknown reactive biogenic VOCs. *Science* **304**, 722–725 (2004). doi:10.1126/science.1094392 Medline

8. R. Holzinger, A. Lee, K. T. Paw, A. H. Goldstein, Observations of oxidation products above a forest imply biogenic emissions of very reactive compounds. *Atmos. Chem. Phys.* **5**, 67–75 (2005). doi:10.5194/acp-5-67-2005

9. T. M. Ruuskanen, M. Müller, R. Schnitzhofer, T. Karl, M. Graus, I. Bamberger, L. Hörtnagl, F. Brilli, G. Wohlfahrt, A. Hansel, Eddy covariance VOC emission and deposition fluxes above grassland using PTR-TOF. *Atmos. Chem. Phys.* **11**, 611–625 (2011). doi:10.5194/acp-11-611-2011

10. M. Hallquist, J. C. Wenger, U. Baltensperger, Y. Rudich, D. Simpson, M. Claeys, J. Dommen, N. M. Donahue, C. George, A. H. Goldstein, J. F. Hamilton, H. Herrmann, T. Hoffmann, Y. Iinuma, M. Jang, M. E. Jenkin, J. L. Jimenez, A. Kiendler-Scharr, W. Maenhaut, G. McFiggans, T. F. Mentel, A. Monod, A. S. H. Prévôt, J. H. Seinfeld, J. D. Surratt, R. Szmigielski, J. Wildt, The formation, properties and impact of secondary

organic aerosol: Current and emerging issues. *Atmos. Chem. Phys.* **9**, 5155–5236 (2009). doi:10.5194/acp-9-5155-2009

11. T. Karl, P. Harley, L. Emmons, B. Thornton, A. Guenther, C. Basu, A. Turnipseed, K. Jardine, Efficient atmospheric cleansing of oxidized organic trace gases by vegetation. *Science* **330**, 816–819 (2010). doi:10.1126/science.1192534 Medline

12. J.-H. Park, A. H. Goldstein, J. Timkovsky, S. Fares, R. Weber, J. Karlik, R. Holzinger, Eddy covariance emission and deposition flux measurements using proton transfer reaction-time of flight-mass spectrometry (PTR-TOF-MS): Comparison with PTR-MS measured vertical gradients and fluxes. *Atmos. Chem. Phys.* **13**, 1439–1456 (2013). doi:10.5194/acp-13-1439-2013

13. A. Jordan, S. Haidacher, G. Hanel, E. Hartungen, L. Märk, H. Seehauser, R. Schottkowsky, P. Sulzer, T. D. Märk, A high resolution and high sensitivity proton-transfer-reaction time-of-flight mass spectrometer (PTR-TOF-MS). *Int. J. Mass Spectrom.* **286**, 122–128 (2009). doi:10.1016/j.ijms.2009.07.005

14. M. Graus, M. Müller, A. Hansel, High resolution PTR-TOF: Quantification and formula confirmation of VOC in real time. *J. Am. Soc. Mass Spectrom.* **21**, 1037–1044 (2010). doi:10.1016/j.jasms.2010.02.006 Medline

15. R. Holzinger, A. Kasper-Giebl, M. Staudinger, G. Schauer, T. Rockmann, Analysis of the chemical composition of organic aerosol at the Mt. Sonnblick observatory using a novel high mass resolution thermal-desorption proton-transfer-reaction mass-spectrometer (hr-TD-PTR-MS). *Atmos. Chem. Phys.* **10**, 10111–10128 (2010). doi:10.5194/acp-10-10111-2010

16. See supplementary materials on *Science* Online.

17. A. Lee *et al*., Gas-phase products and secondary aerosol yields from the photooxidation of 16 different terpenes. *J. Geophys. Res. Atmos.* **111**, 21 (2006). doi:10.1029/2006jd007050

18. S. Fares, R. Weber, J. H. Park, D. Gentner, J. Karlik, A. H. Goldstein, Ozone deposition to an orange orchard: Partitioning between stomatal and non-stomatal sinks. *Environ. Pollut.* **169**, 258–266 (2012). doi:10.1016/j.envpol.2012.01.030 Medline

19. S. Fares, J.-H. Park, D. R. Gentner, R. Weber, E. Ormeño, J. Karlik, A. H. Goldstein, Seasonal cycles of biogenic volatile organic compound fluxes and concentrations in a California citrus orchard. *Atmos. Chem. Phys.* **12**, 9865–9880 (2012). doi:10.5194/acp-12-9865-2012

20. W. Lindinger, A. Hansel, A. Jordan, On-line monitoring of volatile organic compounds at pptv levels by means of proton-transfer-reaction mass spectrometry (PTR-MS) - Medical applications, food control and environmental research. *Int. J. Mass Spectrom.* **173**, 191–241 (1998). doi:10.1016/S0168-1176(97)00281-4

21. J. de Gouw, C. Warneke, Measurements of volatile organic compounds in the earth's atmosphere using proton-transfer-reaction mass spectrometry. *Mass Spectrom. Rev.* **26**, 223–257 (2007). doi:10.1002/mas.20119 Medline

22. E. Ormeño, D. R. Gentner, S. Fares, J. Karlik, J. H. Park, A. H. Goldstein, Sesquiterpenoid emissions from agricultural crops: Correlations to monoterpenoid emissions and leaf terpene content. *Environ. Sci. Technol.* **44**, 3758–3764 (2010). doi:10.1021/es903674m Medline

23. S. Fares, D. R. Gentner, J.-H. Park, E. Ormeno, J. Karlik, A. H. Goldstein, Biogenic emissions from Citrus species in California. *Atmos. Environ.* **45**, 4557–4568 (2011). doi:10.1016/j.atmosenv.2011.05.066

24. R. Atkinson, D. L. Baulch, R. A. Cox, R. F. Hampson, J. A. Kerr, M. J. Rossi, J. Troe; IUPAC Subcommittee on Gas Kinetic Data Evaluation for Atmospheric Chemistry, Evaluated kinetic, photochemical and heterogeneous data for atmospheric chemistry: Supplement V, IUPAC subcommittee on gas kinetic data evaluation for atmospheric chemistry. *J. Phys. Chem. Ref. Data* **26**, 521 (1997). doi:10.1063/1.556011

25. R. Atkinson, Kinetics and mechanisms of the gas-phase reactions of the hydroxyl radical with organic compounds under atmospheric conditions. *Chem. Rev.* **86**, 69–201 (1986). doi:10.1021/cr00071a004

26. K. J. Gill, R. A. Hites, Rate Constants for the Gas-Phase Reactions of the Hydroxyl Radical with Isoprene, α- and β-Pinene, and Limonene as a Function of Temperature. *J. Phys. Chem. A* **106**, 2538–2544 (2002). doi:10.1021/jp013532q

27. S. B. Corchnoy, R. Atkinson, Kinetics of the gas-phase reactions of hydroxyl and nitrogen oxide (NO_3) radicals with 2-carene, 1,8-cineole, p-cymene, and terpinolene. *Environ. Sci. Technol.* **24**, 1497–1502 (1990). doi:10.1021/es00080a007

28. A. C. Nölscher, J. Williams, V. Sinha, T. Custer, W. Song, A. M. Johnson, R. Axinte, H. Bozem, H. Fischer, N. Pouvesle, G. Phillips, J. N. Crowley, P. Rantala, J. Rinne, M. Kulmala, D. Gonzales, J. Valverde-Canossa, A. Vogel, T. Hoffmann, H. G. Ouwersloot, J. Vilà-Guerau de Arellano, J. Lelieveld, Summertime total OH reactivity measurements from boreal forest during HUMPPA-COPEC 2010. *Atmos. Chem. Phys.* **12**, 8257–8270 (2012). doi:10.5194/acp-12-8257-2012